LEVEL

DNA 5119F

DETERMINATION OF SHOCK-ENTRAINED DUST CONCENTRATION FROM PHOTOGRAPHIC RECORDS OF NUCLEAR WEAPON TESTS

Teledyne Brown Engineering

Cummings Research Park

Huntsville, Alabama 35807

DTIC
SELECTED
FEB 2 6 1981
E

30 June 1980

Final Report for Period 1 August 1979—30 June 1980

CONTRACT No. DNA 001-79-C-0316

APPROVED FOR PUBLIC RELEASE;
DISTRIBUTION UNLIMITED.

Prepared for

Director

DEFENSE NUCLEAR AGENCY

Washington, D. C. 20305

81 2 26 070

REPORT DOCUMENTATION PAGE		READ INSTRUCTIONS BEFORE COMPLETING FORM
1. REPORT NUMBER DNA 5119F	2. GOVT ACCESSION NO. AD-A095 504	3. RECIPIENT'S CATALOG NUMBER
4. TITLE *(and Subtitle)* DETERMINATION OF SHOCK-ENTRAINED DUST CONCENTRATION FROM PHOTOGRAPHIC RECORDS OF NUCLEAR WEAPON TESTS		5. TYPE OF REPORT & PERIOD COVERED Final Report for Period 1 Aug 79 – 30 Jun 80
		6. PERFORMING ORG. REPORT NUMBER SD80-DNA-2449
7. AUTHOR(s) Ronald Snow Melvin L. Price John P. Doty		8. CONTRACT OR GRANT NUMBER(s) DNA 001-79-C-0316
9. PERFORMING ORGANIZATION NAME AND ADDRESS Teledyne Brown Engineering Cummings Research Park Huntsville, Alabama 35807		10. PROGRAM ELEMENT, PROJECT, TASK AREA & WORK UNIT NUMBERS Subtask N99QAXAG128-11
11. CONTROLLING OFFICE NAME AND ADDRESS Director Defense Nuclear Agency Washington, D. C. 20305		12. REPORT DATE 30 June 1980
		13. NUMBER OF PAGES 98
14. MONITORING AGENCY NAME & ADDRESS*(If different from Controlling Office)*		15. SECURITY CLASS. *(of this report)* UNCLASSIFIED
		15a. DECLASSIFICATION. DOWNGRADING SCHEDULE

16. DISTRIBUTION STATEMENT *(of this Report)*

Approved for public release; distribution unlimited.

17. DISTRIBUTION STATEMENT *(of the abstract entered in Block 20, if different from Report)*

18. SUPPLEMENTARY NOTES

This work sponsored by the Defense Nuclear Agency Under RDT&E RMSS Code B342079464 N99QAXAG12811 H2590D.

19. KEY WORDS *(Continue on reverse side if necessary and identify by block number)*

Dust concentration	Nuclear sweep-up dust	Visibility threshold
Dust density	Contrast attenuation	
Dust particle size distribution	Microdensitometer	
Dust extinction coefficient	Contrast measurements	
Shock-entrained dust	Visual Range	

20. ABSTRACT *(Continue on reverse side if necessary and identify by block number)*

A technique is developed for deducing the extinction coefficient of shock-entrained dust from measurements of object/background contrast attenuation. The measurements are made from frames of Nevada atmospheric test movies for which object and camera are both enveloped by the dust cloud and the object is at a known distance from the camera. The contrast measurements can be made visually at an instant of time at which the object is at the threshold of visual detection. Alternatively, the measurements can be made on a microdensitometer at general times before or after this threshold occurs.

DD `1 JAN 73` 1473 EDITION OF 1 NOV 65 IS OBSOLETE

20. ABSTRACT (Continued)

The technique is applied to films of several NTS shots to arrive at the extinction coefficient. Existing experimentally determined particle size distribution data for shock-entrained dust is then used in conjunction with the deduced extinction coefficient to arrive at the dust concentration. Possible sources of error are identified, and the reliability of the technique is estimated, although a precise quantification of the error bounds can only be made through a simulation experiment. A preliminary test plan is presented for conducting such an experiment as part of a future HE test.

PREFACE

It is impossible to acknowledge in this space all of the many individuals who contributed to this research effort in technical and managerial capacities or who provided invaluable librarial and secretarial assistance. We would be remiss, however, if we failed to single out for recognition Capt. A. T. Hopkins of DNA for his capable supervision and guidance and Messrs. Warren Dickinson, Richard DeKalb, and Melvin Capps of BMDSCOM whose encouragement and support from the outset made available the opportunity to pursue this novel research. It is hoped that the technique described herein will serve to complement existing methods for gaining information regarding the properties of nuclear-burst-generated dust clouds.

Accession For		
NTIS GRA&I	**X**	
DTIC TAB	☐	
Unannounced	☐	
Justification		
By		
Distribution/		
Availability Codes		
	Avail and/or	
Dist	Special	
A		

1

TABLE OF CONTENTS

TABLE OF CONTENTS (CONTINUED)

LIST OF ILLUSTRATIONS

LIST OF ILLUSTRATIONS (CONCLUDED)

LIST OF TABLES

1.0 INTRODUCTION

The low lying layer of dust created by nuclear bursts over desert-like ground surfaces produces several effects which are of importance to the defense planner. First, this layer, referred to as shock-entrained or sweep-up dust, contributes to the loading of the dust stem which is of importance in considering RV or interceptor erosion, radar propagation disturbance, and radioactive fallout. Secondly, the low lying layer can itself adversely affect propagation of radar and other electromagnetic or optical communication signals. Thirdly, this dust is of concern because it may alter the waveform of the shock wave and because its concentration may be so great as to affect the dynamic load imposed upon a structure.

A newly devised technique* for determining shock-entrained dust concentration through analysis of existing Nevada atmospheric test photographic records is described in this report. Results obtained by application of the technique to s _ected motion picture frames of several nuclear test shots are also presenced.

1.1 BACKGROUND

The extensive Nevada test movie footage has been effectively exploited in the past to arrive at mathematical expressions for the

----

* At the outset of this research the name "Visual Range Technique" was coined. The designation used herein, which better connotes the more general aspects of the method, is "Contrast Attenuation Techn ique".

spatial dimensions of the precursor shock-entrained dust layer as a function of weapon yield, burst altitude, and time. This was accomplished by correlating, for a variety of test shots, measurements of dust layer film images with known burst data and time (Reference 1). In somewhat related investigations (Reference 2) measurements of the height of the thermally generated pre-shock dust layer were made utilizing the Nevada Test Site (NTS) films.

Merely a cursory examination of the NTS photographic data reveals that there exists a large collection of movies produced to record various nuclear effects on a variety of objects. The objects are usually at ranges varying from a few meters to about a hundred meters from the camera. Almost invariably, during or shortly following the observed effect, both the photographed scene and the camera become immersed in a cloud of dust. As the dust is swept to and fro across the field of view by the post-shock winds, objects are alternately rendered visible or obscured by the nonuniform billows. Toward the end of the negative phase the dust cloud approaches uniformity, and the objects become more or less clearly visible, depending on their distance from the camera and on the general level of dust concentration.

These observations of the reduction in visibility of the photographed objects led to the present attempt to express this measureable reduction in terms of the unknown dust concentration and the usually known observer/object distance. This would then allow one to determine the concentration level. Indeed, previous investigations based on this

approach can be found (e.g., Reference 3). Although these studies involved fog as the obscuring medium, and visual measurements were taken at the actual scene and not from photographic replications of the scene, the principles employed are quite applicable to the present problem.

In the cited study an approximate theoretical relationship between the meteorological range (related to the visual range) and the liquid water content of fog was developed. The relationship was later refined (References 4, 5, and 6) to include precise specification of the particle size distribution. In these studies, predicted water content based on observed meteorological or visual range was in good agreement with measured water content, as exemplified in Figure 1.

The visual range is roughly defined as the distance in an attenuating medium at which an object is barely perceptible to an observer. Based on this rough definition, the cited studies may be said to have determined the concentration of the fog by measuring how far the human eye can see into it. Actually, the concept of visual range is derived from the ideas of contrast attenuation and visual threshold (Reference 7) and may be more precisely defined as the distance, under daylight conditions, at which the apparent contrast between an object and its background becomes just equal to the observer's threshold of contrast detection.

In observing an extensive landscape on a hazy day the reader has doubtless observed the phenomenon of contrast attenuation. The photograph of successive mountain ranges shown in Figure 2 clearly depicts
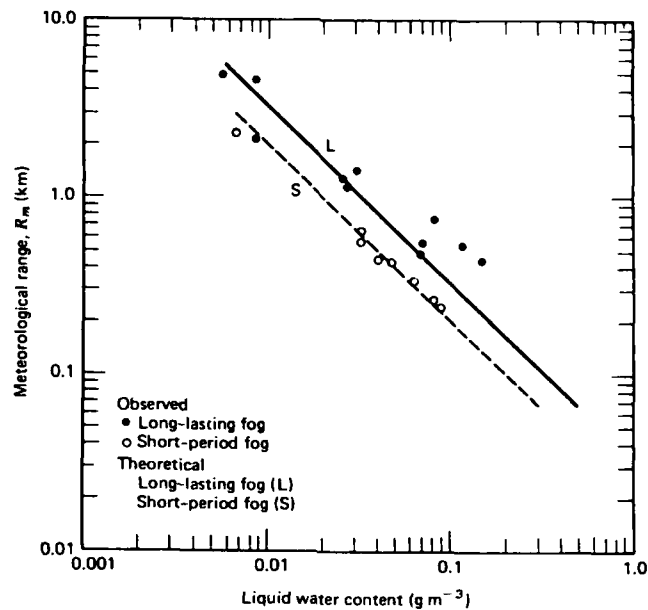
Figure 1. Meteorological range versus liquid water
content of arctic fogs. From Kumai (1973).

the phenomenon. It is observed that the tree covered hills in the fore-
ground are in pronounced contrast with the horizon sky background, whereas
the contrast becomes progressively less pronounced for the more distant
ranges. Contrast attenuation is further demonstrated in the photograph
of Figure 3 for which fog is the attenuating medium. Here, it is seen
that the trees become less darkly contrasted against the light background
as their distances increase until eventually no contrast is detectable.
A tree just at the threshold of detectability would be said to be at its
visual range. For the particular fog in which this photo was taken this
distance was measured to be 45 meters.

The present study has applied the concepts of contrast
attenuation and visual range in analyzing selected Nevada atmospheric test

Figure 3. Example of contrast attenuation caused by fog.

Figure 2. Example of contrast attenuation caused by atmospheric haze.

11

photographic records. In particular, photographs of objects at known distances and under various degrees of obscuration by dust are examined either visually or with the aid of a microdensitometer to arrive at a determination of the level of concentration of the dust. It should be pointed out that the techniques used here are rather crude compared to those involving the sophisticated dust analyzing instrumentation currently employed in high explosive tests. However, it is felt that the visual and photometric approach set forth here is well suited to gain otherwise unobtainable dust concentration information from the photographs of past nuclear tests.

1.2 OBJECTIVES

The objectives of the present study are enumerated below. The respective section of the report which documents the accomplishment of each objective is noted.

1.2.1 Formulation of Theoretical Principles

Although the principles on which this study is based are not original, nevertheless they have never been applied in connection with the determination of dust concentration. Therefore, a brief summary is given in Section 2 of the concepts of brightness contrast attenuation, visual range, particle size distribution, and Mie scattering cross-section as they are applicable in the present context. The theoretical relationships from which one obtains the desired dust concentration in terms of observed contrast attenuation are also presented.

1.2.2   Exhaustive Survey of NTS Films and Associated
             Weapon Test (WT) Documents

The DASIAC catalogue of Nevada atmospheric test films was searched in an attempt to locate all motion picture footage which is relevant to the present shock-entrained dust concentration study. Films were selected based on documented descriptive comments on the objects and action within the field of view as well as furnished quantitative data pertaining to frame rate, time duration of film, and range of cameras and objects from the burst. The quantitative data was considered in conjunction with known time of arrival and spatial extent of the dust layer to select promising footage for further visual examination. Each candidate movie was then viewed to ascertain the degree of obscuration of objects within the field of view in order to determine whether contrast attenuation and/or visual range could be measured at various times following dust arrival.[*]

In addition to the survey of the film archives, the associated weapon test documentation was also searched to obtain parameter values required in performing the dust concentration determinations. The

---

[*] It should be borne in mind that, during the Nevada test series, dust was generally regarded as merely a nuisance to be avoided in performing nuclear effects photography. On occasion, definite steps were taken to alleviate the visibility problems caused by the dust. These included stabilization of the soil in the photographed region and elevation of the cameras well above the ground surface. It should also be mentioned that, since there was little interest in photographing the dust itself, much of the footage showing pronounced obscuration of the test objects was discarded. In view of the present defense interest in nuclear dust these circumstances are unfortunate, especially so now that atmospheric testing is disallowed. In spite of these drawbacks, however, a large number of motion picture sequences were found to exist which can provide dust concentration information when analyzed by the contrast attenuation technique.

requisite quantities include photographic layout geometries, film and framing rate information, and weapon burst parameters. The analysis also required the gathering of data pertaining to size distribution and refractive index of the NTS dust particles.

1.2.3   Performance of a Consistency Check on Contrast
         Attenuation Technique Results

A purpose of the present study was to perform preliminary tests for validating the newly devised technique to gain confidence in its suitability for photographically determining nuclear dust concentration levels. One such test, which was considered essential, was to check the consistency of the dust concentration predictions when the method was applied to films of different shots for which the test conditions were approximately equivalent. The results of this consistency study are presented in Section 3.

1.2.4   Determination of Sensitivity of Dust Concentration
         Predictions to Variations in Particle Size Distribution

It was suspected that the dust concentration determined by the contrast attenuation technique would strongly depend on choice of particle size distribution. A sensitivity both to the shape and the size limits of the distribution has been demonstrated in visual range determination of fog density (References 4, 5, and 6). To ascertain the degree of this sensitivity for the present dust considerations the investigation described in Section 4 was carried out. It was expected that this investigation would provide an indication of the uncertainity in the determined dust concentration levels arising from possible uncertainity in measured particle size distribution.

1.2.5   Microdensitometer Measurements of Contrast
         Attenuation

To complement the determination of dust concentration through
visual detection of threshold contrast (reported in Sections 3 and 4),
contrast measurements were made with the aid of a microdensitometer
(reported in Section 5). One of the purposes of these measurements was
to provide a check on the visual measurements. The other purpose was to
extend the contrast attenuation technique to cases involving general
contrasts below and above visual threshold.

1.2.6   Investigation of Error Sources

In addition to the investigation of the effects of uncertainty
in particle size distribution on the predicted dust concentration, pre-
liminary examinations of other expected sources of error were made as they
were encountered in the study. There are basically three categories
of error sources. These are, 1) uncertainties in contrast attenuation
and threshold associated with the actual viewed scene, 2) inaccuracies
introduced in the photographic replication of the scene, and 3) limita-
tions of the theoretical models which relate the desired concentration to
the measured contrasts. A thorough determination of error bounds of the
contrast attenuation technique will require performance of the experiment
planned in objective 1.2.7.

1.2.7   Development of a Comprehensive Validation Test Plan

To accurately quantify the accuracy of dust concentration
levels predicted by the contrast attenuation technique a detailed plan
of a validation experiment was devised (see Section 6). This experiment

15

is designed to be performed in connection with a future high explosive test. The experiment will determine the accuracy of the technique by comparing dust concentrations deduced from photographically recorded contrast attenuation with those obtained simultaneously using state-of-the-art dust sampling and measuring instrumentation.

2.0 FORMULATION OF THEORETICAL PRINCIPLES

This section presents a summary of the concepts of brightness
contrast attenuation, visual range, particle size distribution, and
Mie scattering cross-section as they pertain to the present dust consid-
erations. Also presented is the theoretical framework for relating
these quantities to permit solving for the desired dust concentration.

2.1   ATTENUATION OF CONTRAST

Consider an observer and an object viewed under daylight
conditions, both immersed in a uniform attenuating particulate medium
as shown in Figure 4. If the object is an ideally black one its image
when observed at close range (i.e., $R = 0$, and no intervening medium)
represents a complete absence of light, and the image is darkly contrasted
against the light background. As the observer moves away from the object
the "airlight" phenomenon causes the object to appear lighter and hence
less darkly contrasted against the background. This phenomenon results
from the scattering of light into the cone of vision from all points in
the particulate medium and the subsequent rescattering of some of this
light, then the line of sight to the object, into the observer's eye.
This latter scattered light reaches the eye from the direction of the
object and has the effect of brightening its image and reducing its contrast.

The brightness contrast, when the object is viewed from a
distance R (called the apparent contrast) is given by

$$C_R = \frac{b_{ob}(R) - b_b}{b_b}$$
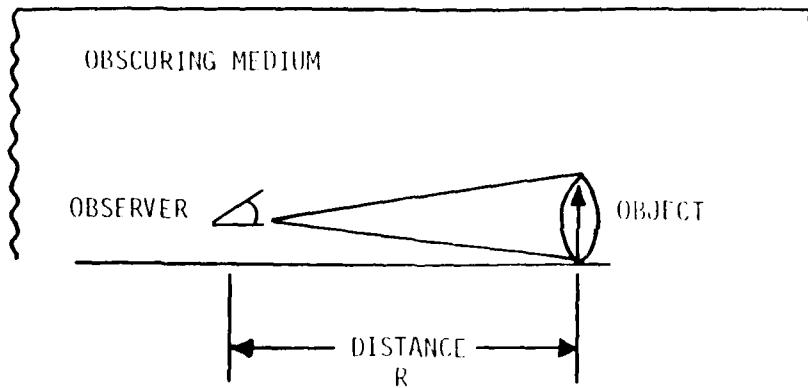
Figure 4.   Object viewed by an observer through
a light attenuating medium.

where $B_{ob}(R)$ is the brightness of the object as measured from the distance
R, and B_{bg} is the brightness of the background. Similarly the brightness
contrast of the object when viewed at close range is

$$C_o = \frac{B_{ob}(0) - B_{bg}}{B_{bg}} , \qquad (2)$$

where C_o is the contrast measured at close range (i.e., the inherent
contrast of the object). We note that, for an ideal black object,
$B_{ob}(0)$ is 0, and C_o is -1.

It is known[*] that the contrast "attenuation" caused by the
medium is given by

$$\frac{C_o - C(R)}{C_o} = 1 - \exp(-\sigma_s R), \qquad (3)$$

[*] This relationship is well established experimentally. Furthermore,
it may be derived theoretically from first principles (see Chapter 4
of Reference 7).

where R is the object distance, and β_s is the scattering extinction coefficient of the medium.* Accordingly, the contrast "transmission" is defined as

$$C(R)/C_o = \exp(-\beta_s R) \quad .$$

(4)

2.2 DETERMINATION OF EXTINCTION COEFFICIENT BY MEASUREMENT OF VISUAL RANGE

As the observer/object distance R is increased the contrast transmission drops in accordance with Equation 4. When the contrast transmission drops to the threshold at which the image is barely distinguishable against the background, then the object is by definition at a distance equal to the visual range V. Under these conditions we have:

$$(C/C_o)_{thresh} = \exp(-\beta_s V),$$

(5)

from which we can calculate the extinction coefficient.

$$\beta_s = \frac{-\ln(C/C_o)_{thresh}}{V}$$

(6)

Thus, if one measures the distance at which he just perceives an object, and if he knows his eye's contrast transmission threshold for the

_____

* If the object is not ideally black then it "emits" some light, and direct beam absorption in addition to scattering of this light by the intervening medium must be taken into account. For the completely black object, however, the contrast attenuation is caused solely by light being introduced into the field of view, and this process involves only scattering. All the cases considered in the present study involved objects which more or less approached blackness, so that only scattering was considered. There is no reason, however, why the method cannot be used for objects having non-zero inherent brightness, as long as the absorption cross section is appropriately introduced.

particular object, he can determine the extinction coefficient of the medium from Equation 6.

Obviously, measurements of visual range by different observers would be expected to differ somewhat because natural eyesight variations result in differences in contrast perception from one individual to another. Tests in which thousands of threshold measurements were made on a large number of individuals give a measure of the statistical variation to be expected (References 7 and 8). In these tests each observer determined the visual range by measuring the distance from a range marker at which he just perceived the marker. Simultaneously, the extinction coefficient of the medium was measured with a transmissometer. Then, from Equation 5 the contrast transmission threshold associated with each measurement by each individual observer was calculated. The thresholds were found to be distributed log-normally as shown in Figure 5. Using the midline between the two sets of measurements one sees that only ten percent of the measured thresholds fall below .015 and only ten percent lie above .067, and the median threshold is .030. We summarize in Table 1 the experimentally determined variation in observers' thresholds and the corresponding variation in the extinction coefficient determined from Equation 6. The foregoing data imply that if a random observer determines visually the visual range for one of the scenes shown in the selected films and employs the expression $\beta_s = 3.5/V$, then eighty percent of the time the true value of β_s would lie approximately within plus or minus twenty percent of the calculated value.
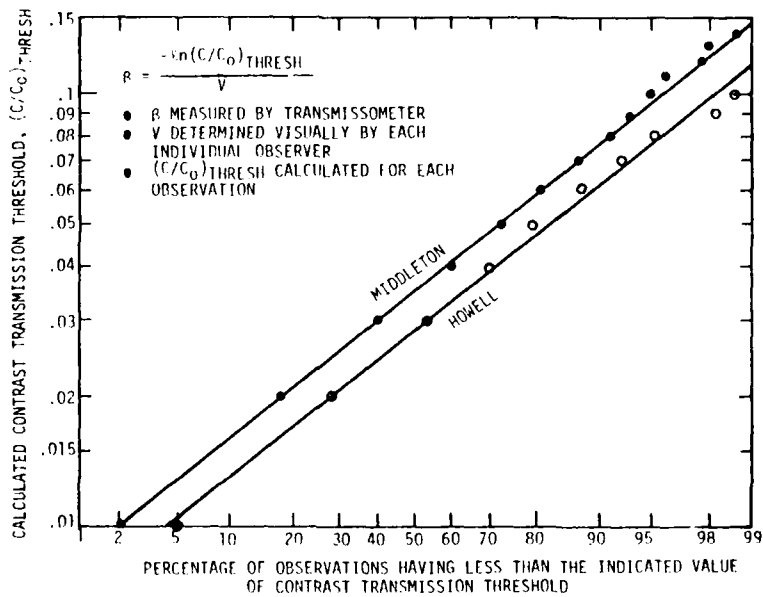
Figure 5. Statistical variation among individual observers' contrast transmission threshold for a black object $(C_o = -1)$.

Table 1. Observed variation in contrast transmission threshold and corresponding variation in extinction coefficient.

$(C/C_o)_{thresh}$		β_s
NOMINAL LOWER LIMIT	.015	4.2/V
MEDIAN VALUE	.030	3.5/V
NOMINAL UPPER LIMIT	.067	2.7/V

It is important to point out that except for very small dark objects and very poor lighting conditions, the threshold distribution shown in Figure 5 is independent of object size and background lighting. Indeed Blackwell (Reference 9) shows this independence to exist for objects whose angular diameter exceeds 200 arc-minutes (approximately equivalent to a dime viewed from one foot away) and for lighting conditions varying from those of noon on a clear day down to one quarter hour after sunset. We mention that the lighting conditions and the object (or rather, film image) sizes encountered in the present study do not exceed these limits.

It should be noted that a possible error is introduced when one makes the visual range determination from a photograph of the scene instead of the scene itself. The differences between the actual visual range and the "photographic" range can arise from three sources. First, a variation from unity of the slope of the emulsion's characteristic curve can result in a difference between the contrast on the photograph and the contrast existing in the actual scene[*]. Second, there is usually some scattered light present in cameras. Addition of this "veiling glare" to the light in the direct image can cause a reduction in contrast. Third, the emulsion has a spectral sensitivity that usually deviates from that of the eye. This fact, coupled with the attenuating medium's possible preferential scattering of certain wavelengths in the regions containing the spectral sensitivity deviations, can alter the contrast.

----

[*] In spite of this alteration in contrast, films with non-unity gamma can still be used to determine the dust extinction coefficient, and hence the dust concentration, as is demonstrated in Section 5.

The exact extent of the effect of these photographically introduced errors on the results obtained in the present dust study can only be determined by duplicating as nearly as possible the experimental conditions which existed in the nuclear test. Duplication of conditions pertaining to attenuating medium, lighting conditions, and cameras and film employed is planned in the high explosive validation experiment described in Section 6. Preliminary to this comprehensive experiment some measurements have been made in the present study which give a rough indication of the magnitude of the difference between visual and photographic range which might exist.

This preliminary experiment involved measurement of the visual range in fog instead of dust. Various objects immersed in this fog were approached by an observer, and the distance at which each object became visible (visual range) was measured to be 45 meters. The object was photographed from this distance using high speed Kodak Tri-X Pan film at f/5.6 and 1/250 second. Photos were also taken at measured increments nearer to and farther from the object. Figures 6 and 7 are photos of a cabin and rail fence taken at the visual range and at 10 meters (22 percent) nearer. The cabin is seen to barely approach the threshold of visibility on the photographic record only when the camera is moved closer by this amount. Similarly, Figures 8 and 9 are photos of a tree taken at the visual range and at 15 meters closer. Here, there is seen to be a 33 percent difference in the visual range and the photographic range. These photos demonstrate that an error could possibly be involved in determining the visual range from photographic records in the present

Figure 6. Cabin photographed from the visual range of
45 m in fog.

Figure 7. Cabin photographed from a distance
10 m less than the visual range.

Figure 8. Tree photographed from the visual range of
45 m in fog.
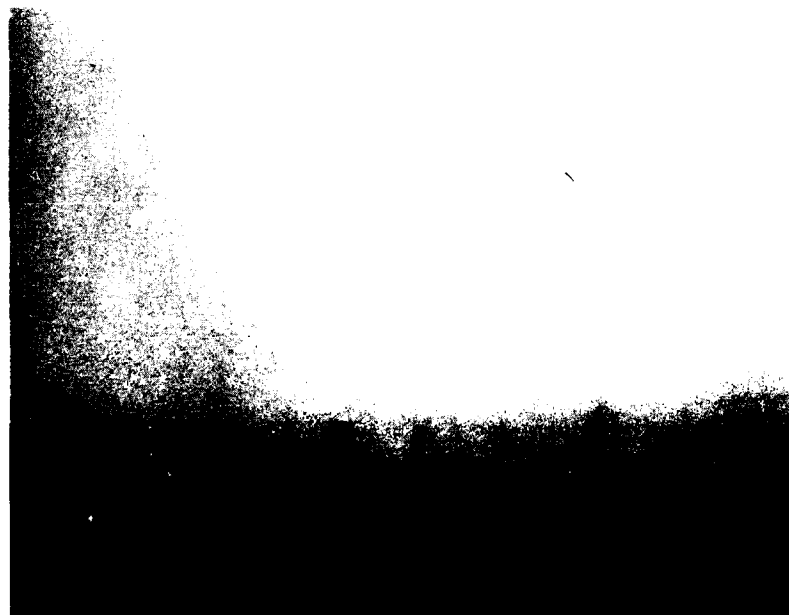
Figure 9. Tree photographed from a distance 15 m
less than the visual range.

dust study. If such an error does exist for dust it would have to be added to the inherent uncertainty associated with visual range measured at an actual scene (Figure 5).

2.3   THEORETICAL RELATIONSHIPS BETWEEN THE EXTINCTION
         COEFFICIENT AND THE DUST CONCENTRATION

Subsection 2.2 demonstrates how the extinction coefficient of the dust can be determined through measurement of the visual range. It is now shown how the concentration of the dust can be calculated from this extinction coefficient.

The scattering extinction coefficient β_s can be expressed in terms of the microscopic scattering cross section σ_s, and the particle size distribution function f as follows:

$$\beta_s = \int_{r_{min}}^{r_{max}} \sigma_s(r,\bar{n},\lambda) N\ f(r) dr \tag{7}$$

Here, $f(r)dr$ is the fraction of particles having radius between r and r + dr, N is the particle concentration (total number of particles per cubic centimeter), and $\bar{n}$ is the complex index of refraction. The smallest and largest particle radii present in the distribution are denoted by r_{min} and r_{max}, respectively.

The cross section for scattering of light of wavelength λ by a particle of radius r can be calculated on the basis of Mie theory. This has been done for spherical particles having the appropriate index of refraction for southwest desert dust (References 10 and 11) and for a wavelength corresponding to the peak of the photopic vision response curve

26

($\lambda = 0.55\mu$).[*] The ratio $Q(r)$ of this calculated cross section to the geometrical cross section is plotted in Figure 10 as a function of particle radius.

We now note that the particle number concentration can be expressed in terms of the mass concentration ρ_m as:

$$N = \frac{\rho_m}{\int_{r_{min}}^{r_{max}} (4/3)\Pi\ r^3\ \rho_g\ f(r)dr}, \tag{8}$$

where ρ_g is the particle "grain" density, assumed here to be 2.6 gm/cm^3 (Reference 13). Substituting this expression into Equation 7 and solving for the desired dust mass concentration, we obtain

$$\rho_m = (4/3)\ \rho_g \beta_s \frac{\int_{r_{min}}^{r_{max}} r^3\ f(r)dr}{\int_{r_{min}}^{r_{max}} Q(r)\ r^2\ f(r)dr}. \tag{9}$$

Equation 9 is employed in Section 3 and 4 to calculate dust mass concentration levels based on visual range determination of β_s using

---

[*] There is no fundamental reason which prohibits generalizing the calculation to include the entire visible spectrum. To effectively exploit this generalization, however, the film response to the various wavelengths would have to be taken into account in equating Equation 7 to Equation 8 when solving for the desired dust concentration. Moreover, the capability exists to calculate the scattering cross section for more realistic irregularly shaped particles (e.g., Reference 12) as opposed to perfectly spherical ones. However, these generalizations are beyond the scope of the present investigation.
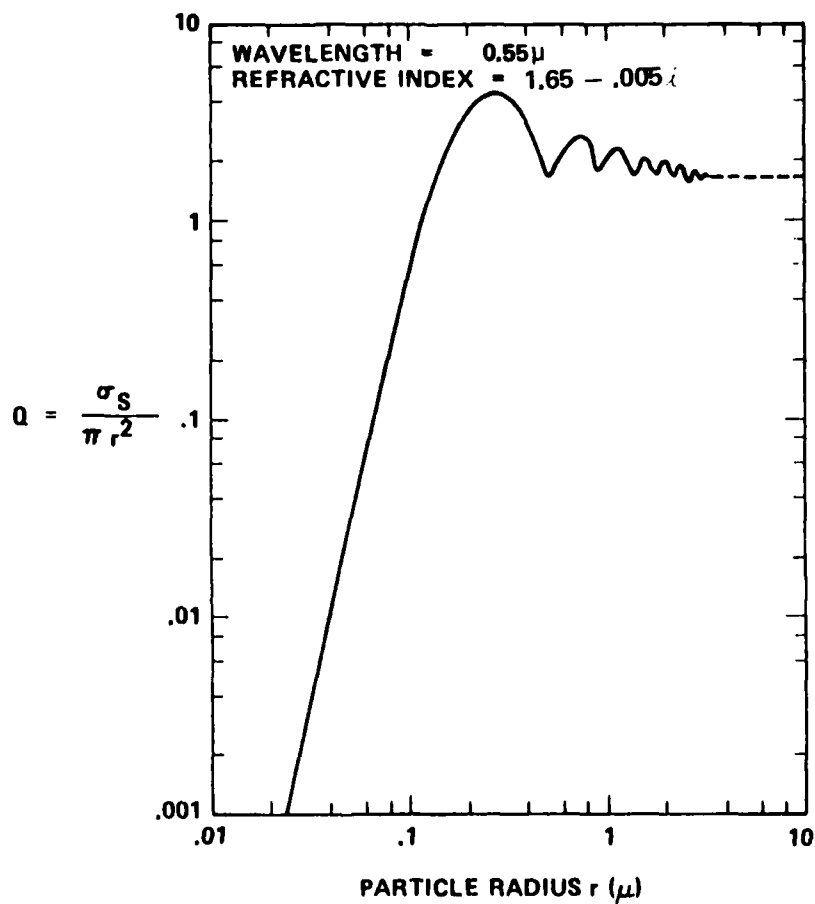
Figure 10. Ratio of Mie scattering cross section to geometrical cross section as a function of particle radius.

Note: This is not to be confused with the commonly plotted $\sigma_t/\pi r^2$ (where σ_t = scattering plus absorption cross section) for which the asymptotic value is exactly 2.

Equation 6 and Table 1. In Section 5 dust concentration is calculated at times other than those at which the viewed object is at the threshold of visibility. In this case β_s is determined by the replacement of the log-contrast-transmission threshold value of 3.5 by the general value measured by the microdensitometer and by the replacement of the specific visual range V by the general camera/object distance R.

3.0 CONSISTENCY TEST OF THE CONTRAST
ATTENUATION TECHNIQUE

To test the consistency of the contrast attenuation technique, films of two different, but roughly equivalent, shots were analyzed. In this particular case a specific aspect of the technique, namely, dust concentration prediction through visual range determination, was tested. In Section 5 one of the selected films (GRABLE) is analyzed further from the more general standpoint which involves concentration predictions at times other than that at which the viewed object is precisely at the threshold of visibility. For considerations of the present section threshold determinations were made visually from the projected image of a positive copy. For the extended study of Section 5 the original negative as well as the positive copy were analyzed with the aid of a microdensitometer, and some observations were made concerning the suitability of employing the copy as regards to fidelity of contrast reproduction.

3.1   TIME OF OCCURENCE OF VISIBILITY THRESHOLD

The two shots under consideration are UPSHOT-KNOTHOLE shot 10 (GRABLE) and TUMBLER-SNAPPER shot 4 (DOG), for which the burst parameters are given in Table 2. Also shown in the diagrams are the burst altitudes, ranges to photographed scene, and burst elevation angles. It is to be noted that the upper diagram corresponds to the lesser yield of 15 KT, whereas the lower diagram corresponds to the greater yield of 19 KT. Some yield-scaling relationship for shock-entrained dust concentration undoubtedly exists which, if known, could be applied to the diagrams to more nearly equalize them.

Table 2. Test conditions for the two shots under consideration.

NTS SHOT	NTS AREA	YIELD (KT)	HOB (M)	GR (M)	GEOMETRY
UPSHOT-KNOTHOLE SHOT 10 (GRABLE)	FRENCH MAN	15	160	1341	6.8°
TUMBLER-SNAPPER SHOT 4 (DOG)	YUCCA	19	317	1829	9.8°

31

On this basis the two shots are seen to be roughly equivalent[*], and
we now demonstrate that at about the same time after shock arrival,
the extinction coefficient and the dust concentration turn out to have
about the same respective values for both shots.

Figure 11 shows two frames from the GRABLE film (EGG 16725)
picturing a boxcar viewed from a camera mounted 5.2 meters above ground.
The boxcar is located 37 meters from the camera. The first frame
corresponds to the instant of shock arrival from the left. The second
frame (number 628 measured from shock arrival) corresponds to a time
after arrival of 9.8 seconds and is the frame adjudged to picture the
lower left quadrant of the end of the boxcar at the threshold of visi-
bility. It will be noted that the contrast varies somewhat from quadrant
to quadrant. The vertical increase in contrast is a systematic variation
which is consistently noted in the films and which is associated with
a decrease in dust concentration with height above ground. Horizontal
variations result from the fact that all the billows in the originally
turbulent sweep-up rarely smooth out into a state of perfectly uniform
density. The lower left quadrant has been singled out for examination
because it is in an appropriate position for comparisons to be made with
the viewed object of the TUMBLER-SNAPPER/DOG film.

---

[*] One should bear in mind that , although an abundance of suitable film
footage exists, it is nevertheless difficult to find exactly equivalent
shots having equivalent camera locations, and most importantly, having
objects viewed from equivalent distances and vantage points. The latter
equivalences are essential in testing whether equal visual ranges are
observed at roughly equal times after shock arrival.

Figure 12 shows two frames from the DOG film (EGC 13396). The dark object selected for observation here is the pair of horizontal black smoke streamers emanating from the pole in the lower left foreground. The camera's vertical vantage point is the same as in the GRABLE film, and the distance to the smoke streamers is 46 meters. The first frame corresponds to the onset of the negative phase and the second pictures the smoke streamers at the threshold of visibility. The frame picturing threshold is number 277 from shock arrival and corresponds to a time of 7.9 seconds.

3.2   DETERMINATION OF INHERENT CONTRAST

To arrive at the extinction coefficient using Equation 6, together with Figure 5, one must know the inherent brightness contrast, C_o, of the viewed object. The reason for this is that the $(C/C_o)_{thresh}$ of Figure 5 is based on observations of an ideal black object ($C_o = -1$), and unless the object observed in the present investigation is ideally black, appropriate adjustment of the ordinate scale of Figure 5 must be made. Determination of C_o would require another photograph of the object taken at close range (i.e., no intervening dust) at exactly the same instant of time that the visibility threshold is detected. The pre-shot view will not suffice, although it does view the object with no intervening dust present. This is because it corresponds to a different time and, hence, to different background lighting conditions. Thus, the background brightness of Equation 2 would differ from that at the time C_{thresh} is observed (Equation 1, with R = V). At any rate, the preceding
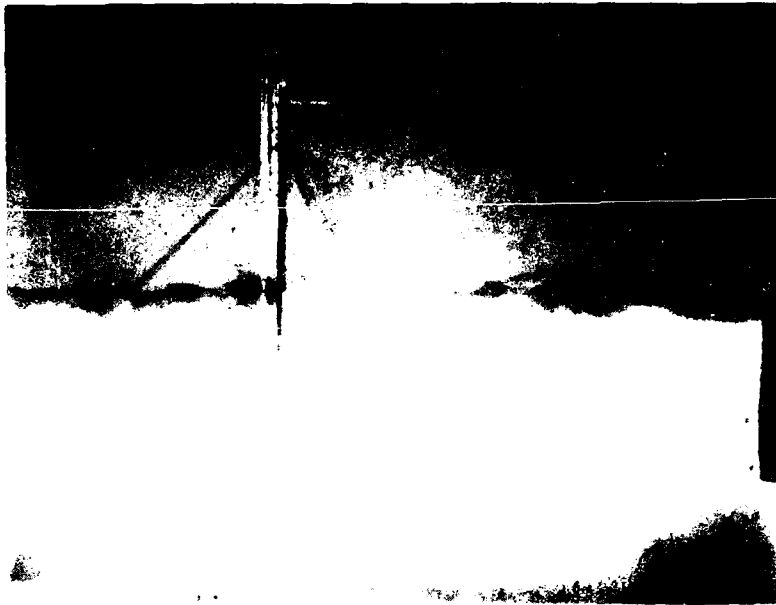
Figure 12. Black smoke streamers in 1-S.DOG test (Film EGG 13596) viewed during negative phase and at 7.9 seconds after shock arrival.

considerations are academic from the present standpoint since we are limiting ourselves in this section to measurements performed with the unaided eye. But the eye can only detect threshold contrast and is unable to assign a value to a non-threshold contrast such as C_o. Therefore, C_o must be deduced from other considerations.

With regard to the T-S DOG film it may safely be assumed that the black smoke approximates an ideal black object sufficiently closely that the value -1 may be adopted for C_o. Concerning the boxcar of the U-K GRABLE film, however, C_o must be deduced from an experiment which fairly closely simulates the nuclear test conditions. This experiment involved measurement of the brightness or, equivalently, the reflectance of ordinary boxcars under background lighting conditions which varied sufficiently widely to encompass the actual test conditions involving the enveloping dust layer.

Preliminary to the experiment, color film footage of railroad equipment involved in the UPSHOT-KNOTHOLE series was viewed with the intent of ascertaining the color of the boxcars used in the black and white GRABLE film presently being considered. It was concluded that the GRABLE boxcars were either of the ordinary rust red variety or were dull black in color.

It will be recalled that the inherent contrast is defined as

$$C_o = \frac{B_{ob}(0) - B_{bg}}{B_{bg}} \, ,$$

(10)

where $B_{ob}(0)$ is the brightness of the object as measured at close range, and B_{bg} is the brightness of the background. But the brightness of the object is simply

$$B_{ob}(0) = R_{ob}B_{bg} \; , \tag{11}$$

where R_{ob} is the reflectance of the object. Thus, by substitution we have

$$C_o = R_{ob} - 1 \quad . \tag{12}$$

This equation was employed in conjunction with measurements of R_{ob}, performed on black and rust red boxcars, to determine the appropriate C_o to use in analyzing the GRABLE film.

The experiment was conducted as follows. A freight yard was visited around dusk on a clear day, and suitable boxcars were selected. Measurements of the brightness of the boxcars were made at various times shortly preceding and following sunset. The instrument employed was a silicon photodiode photometer ("spotmeter") having a one-degree view angle. Simultaneously, measurements were made of the background, which in this case was the sky. For calibrating the instrument scale simultaneous measurements were performed on standard Kodak 18 percent (grey) and 90 percent (white) reflectance test cards. As check points, measurements on a piece of black velvet cloth mounted on the boxcar were included. This cloth is known to very closely approximate an ideal black object ($R_{ob} = 0$).

The value of C_o for the rust boxcar was determined graphically as shown in Figure 13. Spotmeter readings of the sky were plotted at the 100 percent reflectance level. This is because the sky, being the sole source of light, may be treated as a perfect reflector in the present context. The spotmeter readings for the standardized reflectance cards were plotted at their respectively known 90 percent and 18 percent levels. These three sets of points defined straight lines on a log-log grid. Extrapolation of the lines allows one to locate the reflectance associated with spotmeter readings of the boxcar. The reflectance of the rust boxcar was found to be about 8 percent, and measurements on the black boxcar gave essentially the same result. This value of reflectance corresponds to a C_o value of -.92. As a check on the procedure, the reflectance associated with the spotmeter readings of the black velvet was determined. As expected, this reflectance turns out to be very nearly zero (0.3 percent).

3.3   DETERMINATION OF EXTINCTION COEFFICIENT AND DUST CONCENTRATION

Employing Equation 6, Figure 5, the visual ranges deduced from the films, and C_o values of -1 and -0.92 for the smoke streamers and boxcar, respectively, we obtain the values of extinction coefficient shown in Table 3. Here, the median value for $(C/C_o)_{thresh}$ given in Table 1 has been employed.

We now employ Equation 9 and the just obtained values of extinction coefficient to calculate the dust concentration. For these calculations a lognormal particle size distribution is used which has a median radius 0.61μ, a standard deviation of 0.94, and particle radius
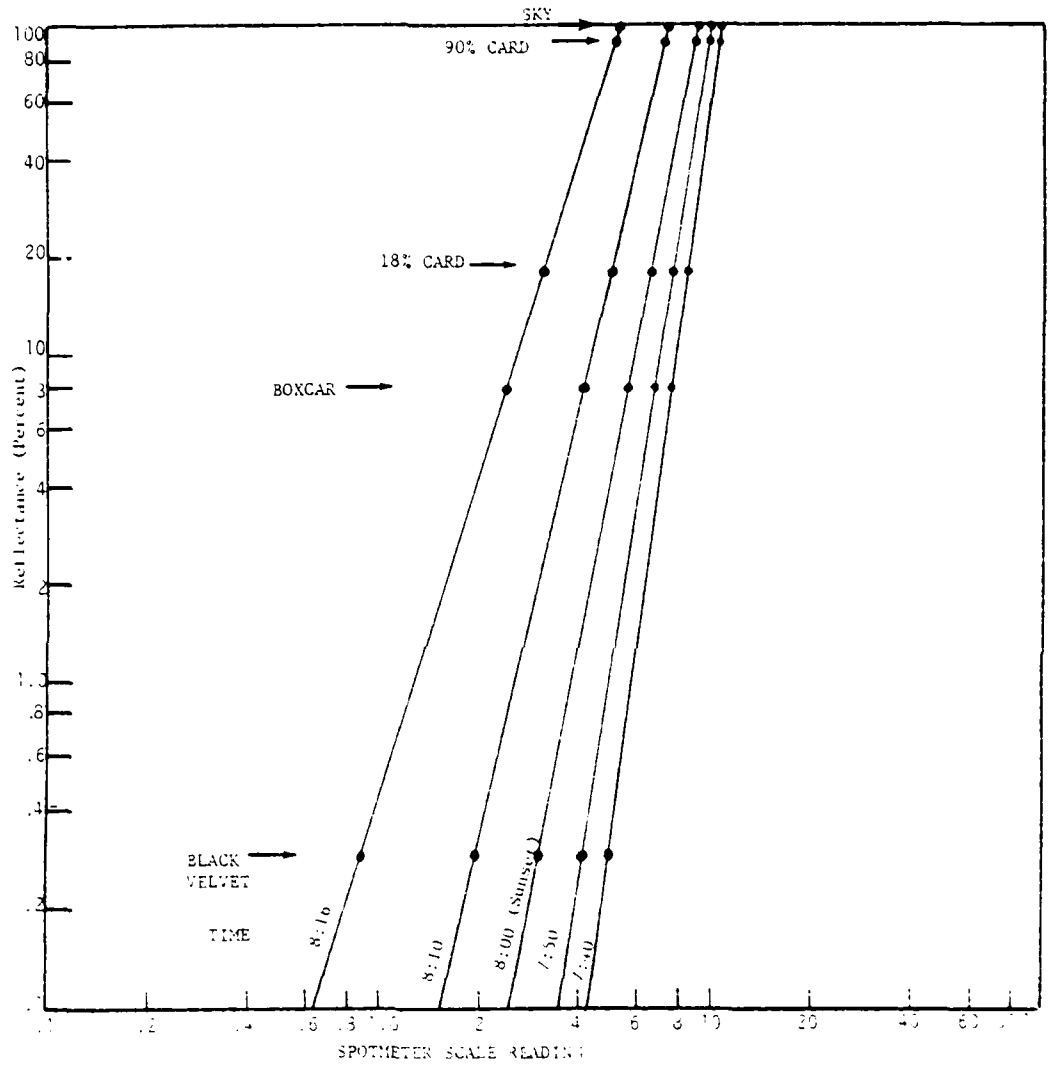
Figure 13. Graphical determination of boxcar reflectance

limits of 0.2 and 25μ. These experimental data, obtained in the TEAPOT/MET shot, are discussed in Section 4. The resulting dust concentration levels at the times indicated are shown in Table 3. It is apparent that the results for the two test cases agree sufficiently closely to establish the consistency of the approach. The slight deviation is certainly within the range one would expect as a result of the known dissimilarities of the two cases.

Table 3. Measured visual range and calculated extinction coefficient and dust concentration for the two test cases.

NTS SHOT	TIME AFTER SHOCK ARRIVAL (SEC)	VISUAL RANGE (M)	EXTINCTION COEFFICIENT (CM^{-1})	DUST CONCENTRATION (GM/CM^3)
UK-GRABLE	9.8	37	9.2×10^{-4}	11.6×10^{-7}
TS-DOG	7.9	46	7.6×10^{-4}	9.5×10^{-7}

4.0 SENSITIVITY OF DUST CONCENTRATION PREDICTIONS TO
VARIATIONS IN PARTICLE SIZE DISTRIBUTION PARAMETERS

The particle size distribution assumed for the dust particles figures prominently in the expression for the mass concentration of the dust (Equation 9). Therefore, it is of interest to investigate how sensitive the calculation of the concentration is to variations in the distribution. This investigation is undertaken in this section in connection with the dust concentration level calculated by visual range determination for the TUMBLER-SNAPPER/DOG shot as recorded in DASIAC film number F1481, (Produced by the U.S. Forest Service).

Selected frames from this movie are shown in Figure 14. The viewed object under consideration is the tree that remains standing after shock arrival. It is known to be 49 meters from the camera, and both tree and camera are 1463 meters from ground zero. At a time of 26 seconds after shock arrival the tree is just at the threshold of visibility. Thus, at this instant of time the visual range in the dust cloud is 49 meters.

The reader has perhaps observed that the burst/camera/object geometry for this film is fairly similar to that of the T-S/DOG film examined in Section 3. However, the times at which threshold occurs are found to be quite different. There are two reasons for this apparent discrepancy. First, in the present film the camera is mounted much closer to ground level than in the previously analyzed film. Secondly, the time of threshold in the present film is determined after the obscuration has peaked and has begun to lessen. But in the previous case,

(a) Pre-shot view
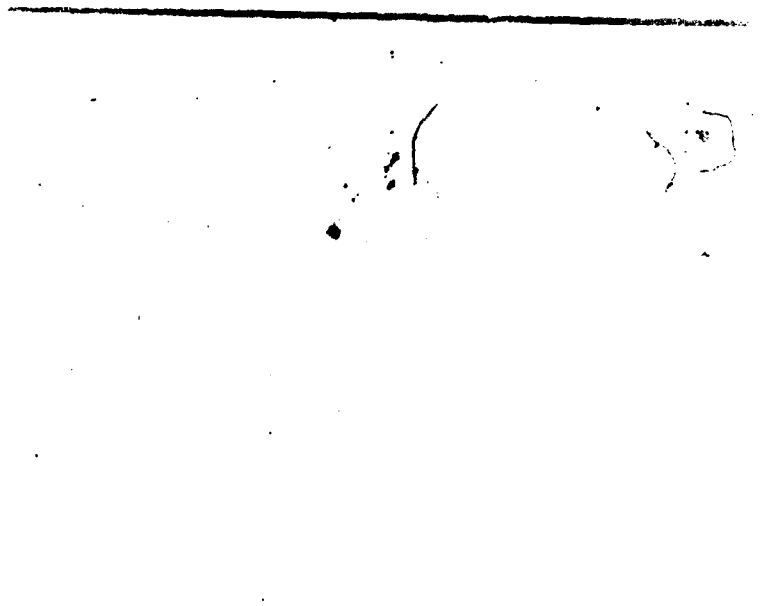
(b) Shortly after
shock arrival
(burst to
right)

Figure 14. Selected frames from TUMBLER-SNAPPER/DOG
film (DASIAC Number F1481).

42
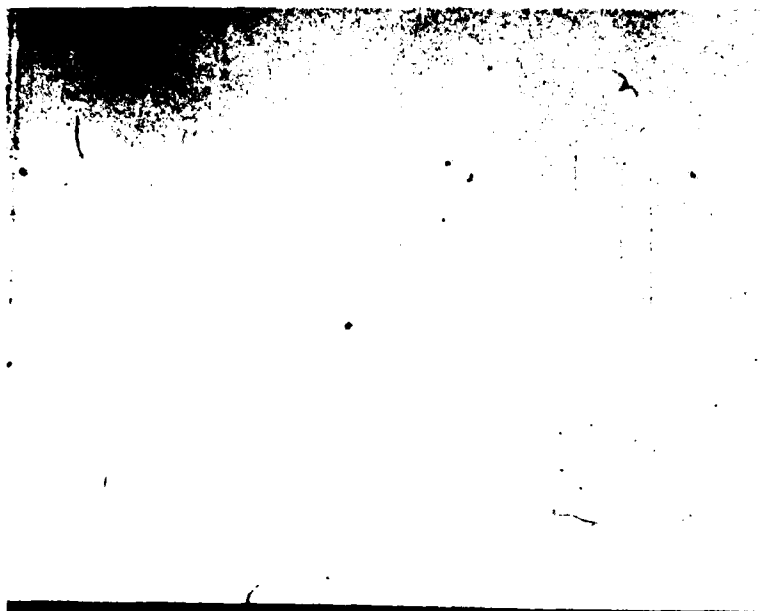
(c) Total obscuration
(Frame 400, t =
12.5 sec after
shock arrival).

(d) Tree at visual
threshold (Frame
840, t = 26 sec
after shock
arrival).

Figure 15. Selected Frames from RUMBLER-SNAPPER DOG
Film (DASIAC Number FI-81), Continued.

48
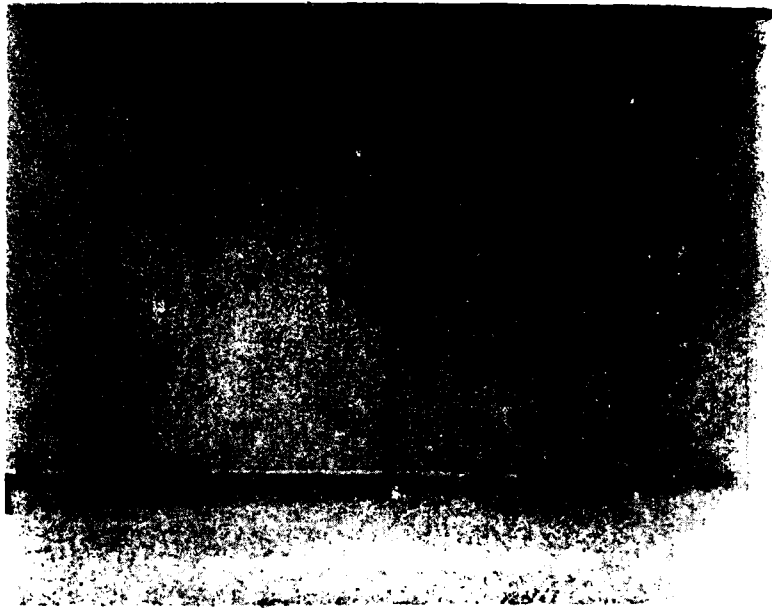
(e) Airplane at visual threshold (Frame 2169, t = 68 sec after shock arrival).

(f) Mountains on left at visual threshold (Frame 6509, t = 203 sec after shock arrival).

Figure 14. Selected frames from TUMBLER-SNAPPER/DOG Film (DASIAC Number F1481), Continued.

time of threshold was determined before obscuration had peaked and was still increasing. The much lower camera in the present case is looking early through very dense dust and, consequently, the tree is obscured very soon after shock arrival. One must wait until the dust has thinned out considerably before visibility of the tree is restored.

Using then the visual range of 49 meters, an appropriate value of C_0 for the tree, and the data in Figure 5, one can obtain the value of the extinction coefficient of the dust at 26 seconds. One can then investigate the sensitivity of the dust concentration predictions to particle size distribution variations by employing different choices of this distribution in Equation 9.

The value of C_0 for the tree was deduced from spotmeter measurements on a pine tree in an experiment like the one involving the boxcars described in Section 3. The values obtained were -0.85 for the branches and -0.88 for the trunk. We will select the latter value for use here although the true value for the tree in the film is probably somewhat closer to -1 due to charring caused by the thermal pulse. With $C_0 = -.88$ and $V = 49m$ we obtain for the extinction coefficient an expected (median) value of 6.9×10^{-4} cm^{-1} with the usual nominal error bounds of ± 20 percent applying due to variations in observer contrast threshold.

In the present parameter sensitivity study the particle size distribution to be considered first is that determined experimentally in the TEAPOT/MET test shot. This shot, which was detonated at Frenchman Flat, had a yield of 22 KT and a burst altitude of 122 meters. Samples of dust entrained by the shock wave were collected at elevations of

1 and 3 meters and at distances from ground zero ranging from 600 meters
to 900 meters. The particle size distribution, averaged over all
collecting stations, was found to be lognormal* in shape with a number
median radius of 0.61μ, a mass median radius of 7.5μ, and a standard
deviation of 0.94 (Reference 14). As far as the present authors have
been able to ascertain, these data constitute the only particle size
distribution measurements reported in connection with shock-entrained dust
generated by nuclear bursts. Reference 14 does not specify the lower
and upper radius limits of the sampled particles r_{min} and r_{max}. But
from the quantities supplied, together with the definitions of the
distribution, number median, and mass median, two equations can be derived
from which these limits may be determined uniquely to be r_{min} = 0.2μ,
and r_{max} = 25μ.

---

*The definition we are using for the (cumulative) lognormal distribution
and its associated parameters is as follows:

$$\frac{1}{\sqrt{2\pi}} \int_{-\infty}^{y} e^{-t^2} dt = \frac{1}{2} \left[1 + erf(y) \right],$$

where $y = \dfrac{\ell n(r/r_0)}{\sqrt{2}\sigma}$, and r_0 and σ are the median radius and standard

deviation, respectively.

Using the TEAPOT/MET size distribution and the previously determined extinction coefficient, we calculate from Equation 9 the dust concentration at 26 seconds after shock arrival. The value obtained is $5.6 \cdot 10^{-7}$ gm/cm^3 as shown as the first entry of Table 4. The first parameter variation considered is shown in the second entry. Here, the maximum particle radius was increased drastically while at the same time σ was altered to preserve the number and mass medians measured in MET. It is seen that this variation produces only a small change in dust concentration. Next, the distribution shape was arbitrarily changed to two exponential forms commonly found in nature (shown in the next two entries). At the same time the lower and upper radius limits were modified to preserve the MET median radius data. Both exponential distributions are seen to give significantly lower dust concentrations than do the lognormal distributions. For the final parameter variations considered we arbitrarily adopt the lognormal distribution measured from samples of thermally produced pre-shock dust collected in the T-S/DOG test shot (Reference 15, page 49). The size distribution of dust produced by thermal blowoff is obviously expected to differ greatly from the distribution of dust generated by the shock entrainment mechanism. We consider it here only for purposes of dust concentration sensitivity analysis. This pre-shock dust distribution, shown as the last entry, yields a dust concentration value which is more than an order of magnitude lower than that predicted with the MET lognormal distribution.

Obviously, only a small set of an unlimited number of possible size distribution variations has been considered. From

Table 4. Sensitivity of dust concentration calculations
to variations in particle size distribution.

SIZE DISTRIBUTION ASSUMPTIONS	CALCULATED DUST CONCENTRATION (10^{-7}GM/CM^3)

TEAPOT/MET SHOCK ENTRAINED DUST MEASUREMENTS
  NUMBER MEDIAN RADIUS   =   .61.
  MASS MEDIAN RADIUS = 7.5.	

LOGNORMAL (σ = .94) MIN r = .2. MAX r = 25.	8.6
LOGNORMAL (σ = .91) MIN r = .2. MAX r = 100.	8.0
$r^{-3.5}$ MIN r = .56. MAX r = 23.	1.2
r^{-4} MIN r = .48. MAX r = 116.	1.7

TUMBLER-SNAPPER/DOG PRESHOCK DUST MEASUREMENTS
  NUMBER MEDIAN RADIUS = .031.
  σ = 1.5	

LOGNORMAL MIN r = .01. MAX r = 25.	0.7

those variations made, however, it is apparent that dust concentration results are quite sensitive to the size distribution assumed. This is to be expected since Equation 9 makes it apparent that there is a complex interplay between the third moment of the distribution (cumulative mass between the limits) and the second moment (cumulative area). The influence of this latter term is further complicated by its convolution with the widely ranging and fluctuating Q of Figure 10. This is not to imply that great uncertainty exists in the results obtained by the contrast attenuation technique. This would be so only if the originally assumed MET distribution were suspect, and there is no reason to adopt this position.

In this connection it might be argued that it is inappropriate to use the TEAPOT/MET particle size distribution in calculations of T-S/DOG dust concentration, since the latter shot occurred at a different location of the test site, namely Yucca Flat, which might be expected to have different dust properties. It will be recalled, however, that this choice of particle size distribution led to consistency between measured extinction coefficients for the U-K/GRABLE (Frenchman) and T-S/DOG (Yucca) films analyzed in Section 3. This fact, considered together with the connection between extinction coefficient and particle size distribution (Equation 7) strongly implies that the distribution is essentially the same in both locations.

5.0 MICRODENSITOMETER MEASUREMENTS OF
CONTRAST ATTENUATION

In Sections 3 and 4 the extinction coefficient and the corresponding dust concentrations were arrived at for a particular time through the determination of the visual range in the dust at that time. In the present section the extinction coefficient and concentration will be determined at general times other than that at which the object under examination is at the threshold of visibility. This will be done with the aid of measurements of general contrast attenuation performed on a microdensitometer.

5.1   INSTRUMENTATION AND PROCEDURE

The measurements were performed on the Marshall Space Flight Center IDAPS (Image Data Processing System) which was developed for Skylab experiment analysis. The IDAPS hardware consists of the following items:

1)   Film scanner[*]

2)   Terminal minicomputer

3)   Interactive display and control[*]

4)   Hard copy devices[*]

5)   Host computer

The film scanner has a scan aperture of 35µ and can perform integration at four levels of precision to obtain progressively enhanced signal/noise

-----

[*] See Figure 15
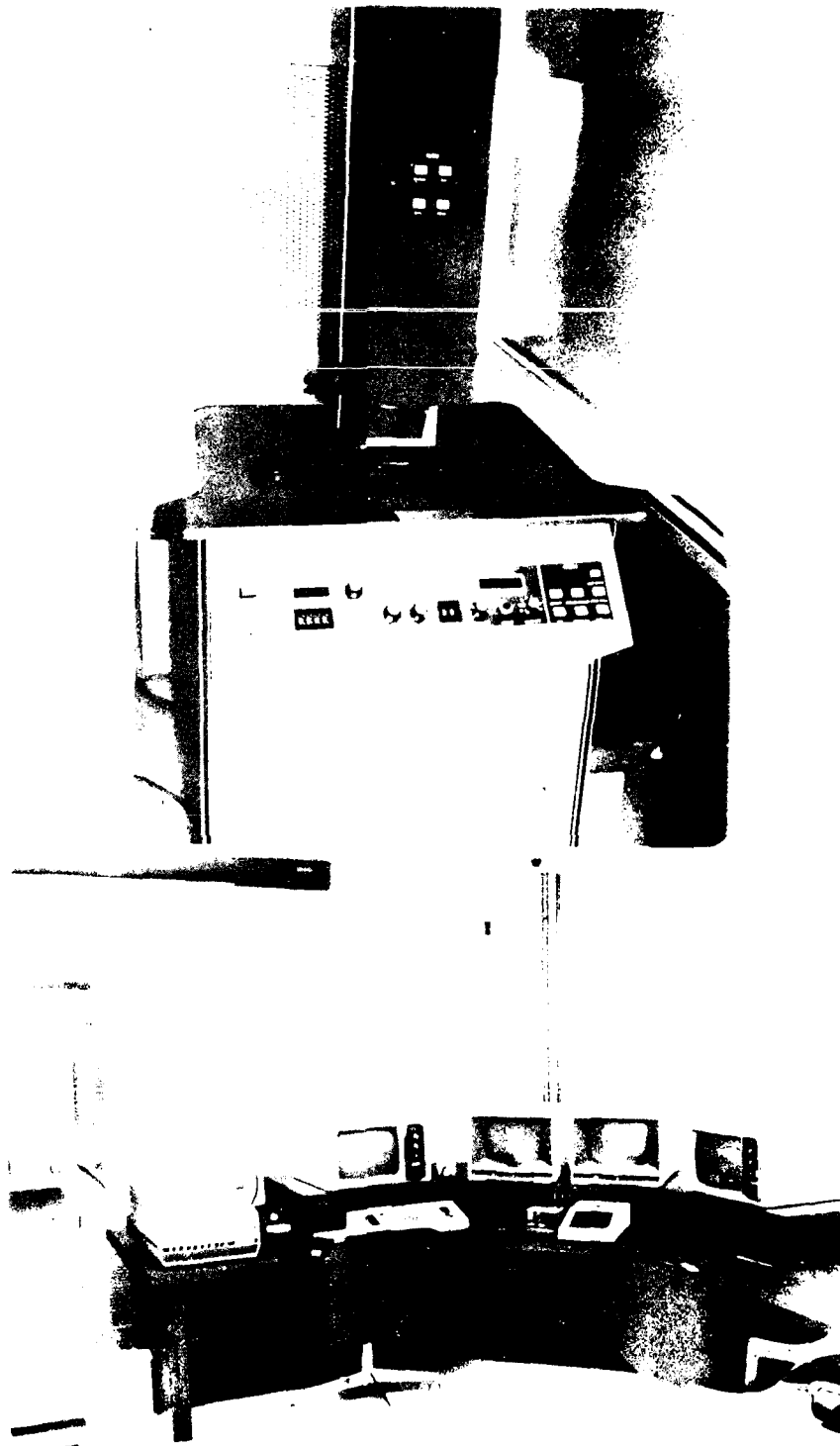
Figure 15. Instrumentation employed in the microdensitometric analysis of film image contrast variations.

ratios from 20 db to 46 db. The precision level adopted for the present measurements corresponds to S/N of 40 db.

An example of a hard copy image display and data readout is shown in Figure 16. The user defines rectangular areas of the object over each of which the instrument will average the transmittance and provide a numerical value for the corresponding average brightness. An absolute brightness level calibration is not required in the present study since only brightness ratios are needed to determine contrast. The rectangle to the right was implaced to obtain an average brightness level over the lower left quadrant of the end of the boxcar. The rectangle to the left was implaced to obtain the average background brightness level. The readout on the left corresponds to the boxcar rectangle and gives in histogram form the frequency of occurence of brightness levels associated with each elemental area in the scan. An elemental area is 5 pixels x 5 pixels, where a pixel is 17.5μ. The minicomputer then computes from this distribution the mean brightness, seen here to have the value 165. The corresponding value for the background was 178.

From the definition in Equation 1 the contrast observed from a distance R (37 meters in this case) is found to be

$$C(R) = \frac{B_{ob}(R) - B_{bg}}{B_{bg}} = \frac{B_{ob}(R)}{B_{bg}} - 1 \tag{13}$$

$$= \frac{165}{178} - 1 = -.0730 \qquad .$$

Using the value of $-.92$ for C_o, determined in Section 3, one can solve Equation 4 for the extinction coefficient to obtain the value $\Gamma_s = 6.8 \times 10^{-4}$ cm^{-1}. Substituting this value into Equation 9 and employing
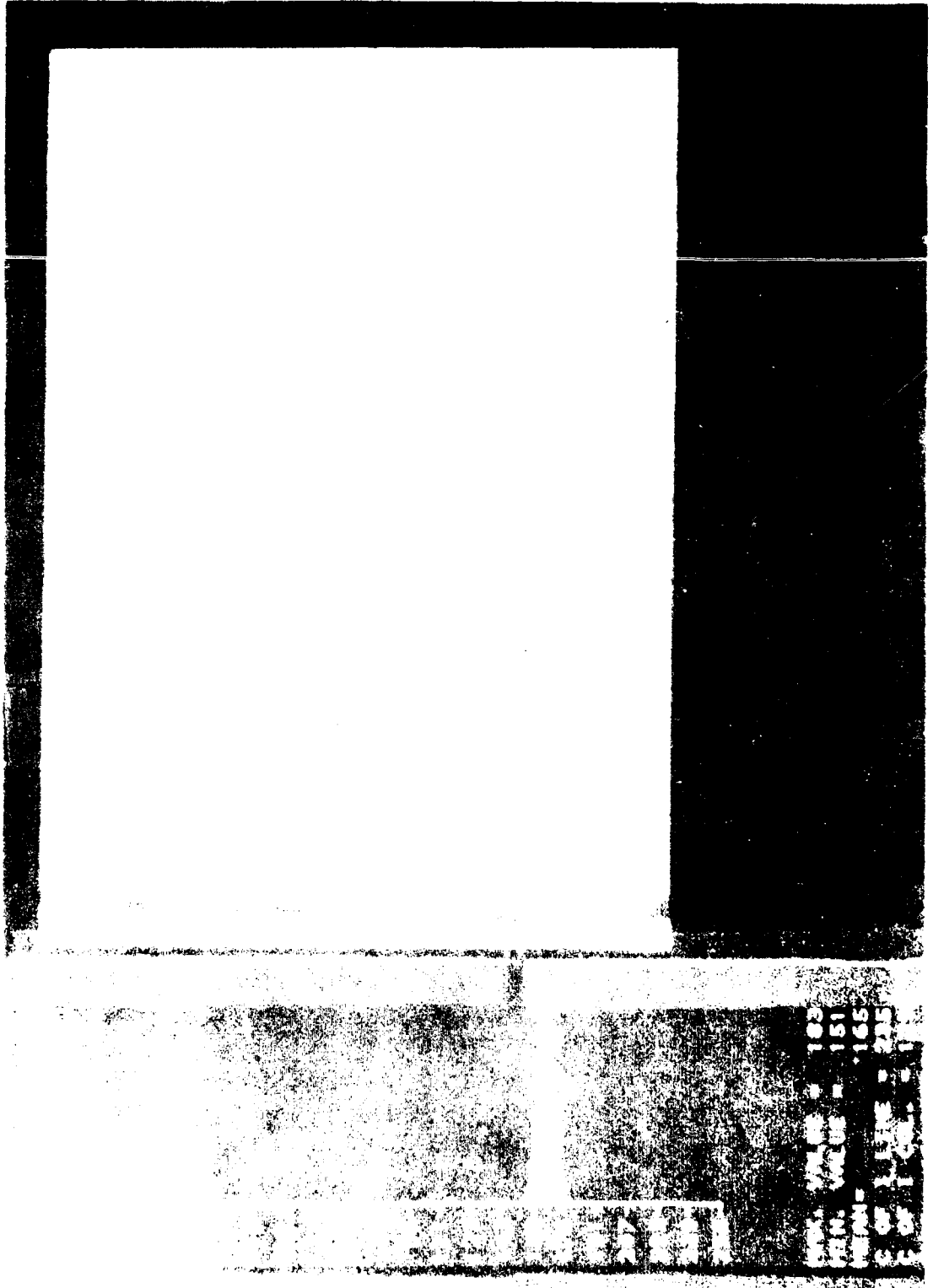
Figure 16. Image under examination as it appears on instrument screen with associated tile density readout.

the TEAPOT/MET particle size distribution presented in Section 4, one obtains a dust concentration of 8.6×10^{-7} gm/cm^3.

At this point a deficiency of IDAPS, which has an impact on the results obtained here, should be mentioned. Each elemental film area is assigned an integral grey value lying between 0 and 255, the specific value depending on the measured transmittance of the particular elemental area. The minicomputer properly averages these integral values over the designated rectangle. However, the software routine is such that this average is rounded off to the nearest integer before being displayed on the screen. Unfortunately, time was not available to modify the software so as to allow retrieval of one or more extra digits.

Thus, error bars had to be assigned to each measured brightness and to each subsequently calculated contrast, extinction coefficient, and dust concentration. For the preceeding example these error limits are determined as follows:

$$C_{lower} = \frac{165.5}{177.5} - 1 = -.0676$$

$$C_{upper} = \frac{164.5}{178.5} - 1 = -.0784 \; , \tag{14}$$

with corresponding lower and upper limits being calculable for the C dependent quantities ε_s and F_m. This round-off error becomes particularly bothersome when the values of B_{ob} and B_{bg} are fairly close together and are in the tens range (i.e., rounded of to a two-digit integer). It should be emphasized that these errors arise from a rectifiable deficiency of the instrument used in the present study, and the resultant uncertainties in the calculated quantities should not be attributed to the contrast attenuation technique itself.

5.2   MEASUREMENTS AND CALCULATIONS

Microdensitometer measurements were performed on selected frames of two U-K/GRABLE movies. The first film analyzed was EGG 16725 which was previously examined in Section 3 in connection with visual determination of extinction coefficient and dust concentration. This film was shot from camera A as shown in Figure 17. The second film considered was EGG 16726 which views the same boxcar during the same time period but from camera B.

Figure 18 shows the shock arrival frame and the selected successive frames of EGG 16725 for which contrast measurements were made. Note that the boxcar end is conveniently divided into quadrants. Measurement of brightness contrast averaged over each quadrant or pairs of quadrants separately allows investigation into the nonuniformity of the dust cloud. Care was taken not to include in a rectangle any portions of the light cross or letter "P" on the boxcar. Inclusion of these light regions is not appropriate when using the C_o value of -.92 and will lead to erroneous results.

Figure 19 shows the extinction coefficient as a function of time after shock arrival as calculated from contrast measurements performed on film EGG 16725. Corresponding results for dust concentration can be obtained from these curves by application of the multiplicative constant noted. Measurements were performed on the negative original (obtained from DNA Field Command) as well as on a positive copy (obtained from DASIAC). It is seen that the copy consistently yields slightly higher values of extinction coefficient than the original. The lower two sets
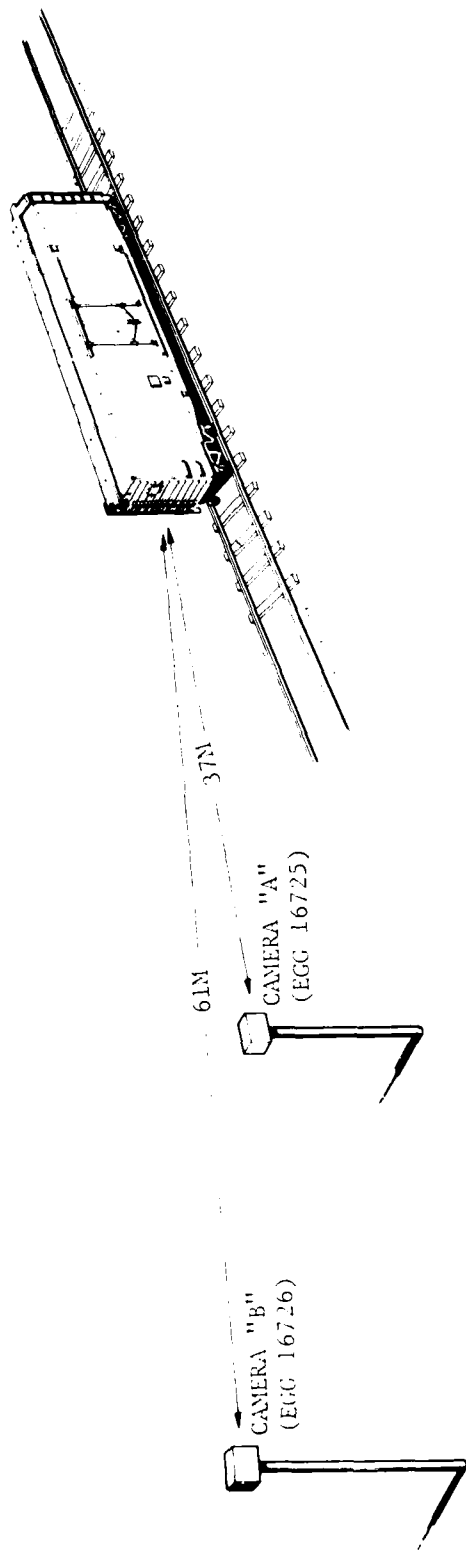
Figure 17. Layout of cameras and viewed boxcar for films EGG 16725 and EGG 16726 of shot GRABLE.

CAMERA "A" (EGG 16725)

CAMERA "B" (EGG 16726)

61M

37M

(a) Shock arrival
(Frame 0, t = 0)

(b) Frame 400,
t = 6.3

Figure 18. Frames of Film USC 16/25 which picture
GRABLE boxcar as viewed from Camera A
at selected times
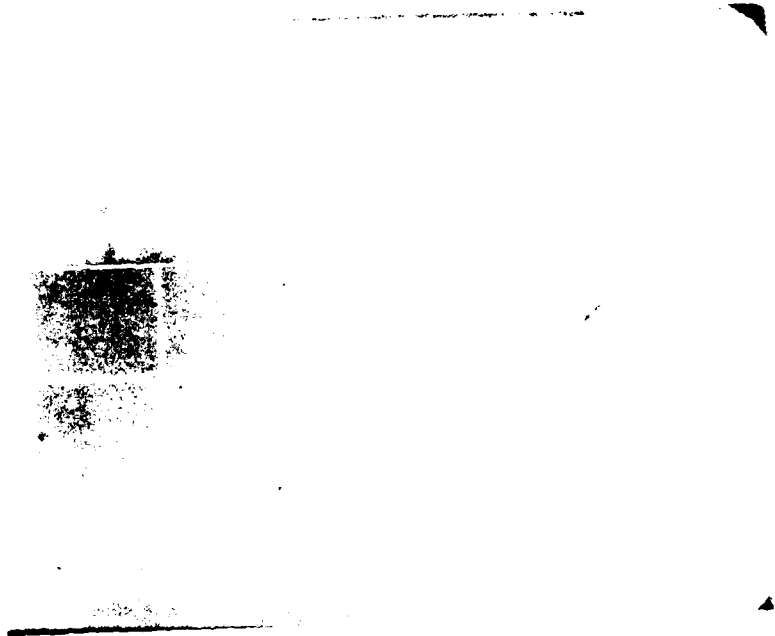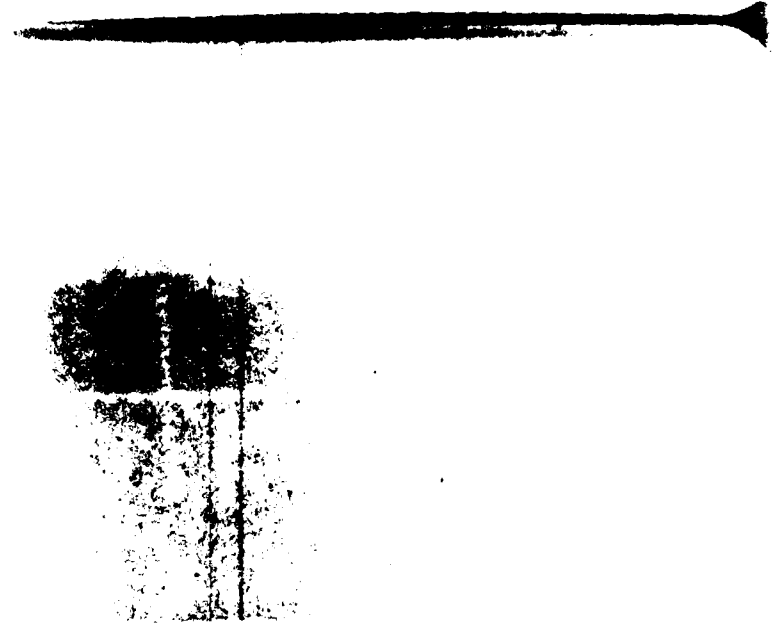
(e) Frame 600,
t = 9.4 sec

(f) Frame 628,
t = 9.8 sec

Figure 18. Frames of Film 1CC 16725 which picture
CRADLE beacon as viewed from Camera A
at selected times (continued).

64
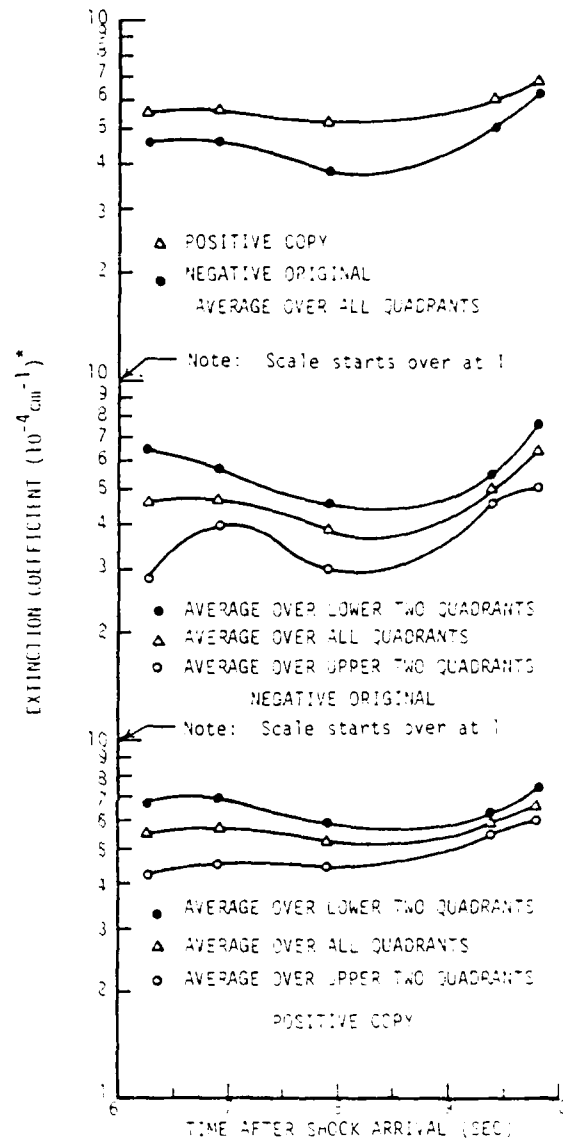
Figure 19. Extinction coefficient of dust based on microdensitometer measurements of contrast performed on boxcar image in GRABLE shot (Film EGG 16725).

*NOTE: Dust concentration $(GM/CM^3) = 1.26 \times 10^{-3} \times$ extinction coefficient (based on Equation 9 with TEAPOT/MET particle size distribution).

of curves demonstrate the expected tendency toward decreasing concentration and extinction coefficient with increasing height above ground. The middle set of curves (original) are seen to be somewhat wider spread than the lower set (copy). This is because the round-off error bounds were greater for the original (on account of the two-digit difficulty mentioned earlier) and because, in addition to the quadrant averaging noted, averaging was also performed over these bounds. The tendency of the curves in the two lower sets to become compressed together at later times demonstrates the gradual approach toward uniform concentration in the dust cloud.

Additional data points were gathered for corroborating the values of extinction coefficient and dust concentration obtained from measurements performed on film EGG 16725. The first set of these additional points were obtained from EGG 16726 through measurements of contrast of the same areas of the boxcar seen from camera B at the same times. As before, Equation 4, with $C_o = -.92$, was employed to solve for the extinction coefficient. However, in this case R is now 61 meters instead of 37 meters. Figure 20 shows the boxcar at the instant of shock arrival as viewed from camera B. Note that camera A appears in the foreground. Contrast measurements were made on the original at 6.3 and 7.9 seconds after shock arrival and on the copy at 6.9 and 7.9 seconds. Calculated extinction coefficient values corresponding to these measurements for the lower left boxcar quadrant are denoted by squares in Figure 21. They are seen to be in good agreement with the values obtained from EGG 16725, which are denoted by circles.

Still further data points were obtained by applying measurements from EGG 16725 and EGG 16726 in combination. Here, a slightly different

Figure 30. Frame of Film LCG 16726 which pictures
CRADLE boxcar as viewed from Camera 8
at the instant of shock arrival.
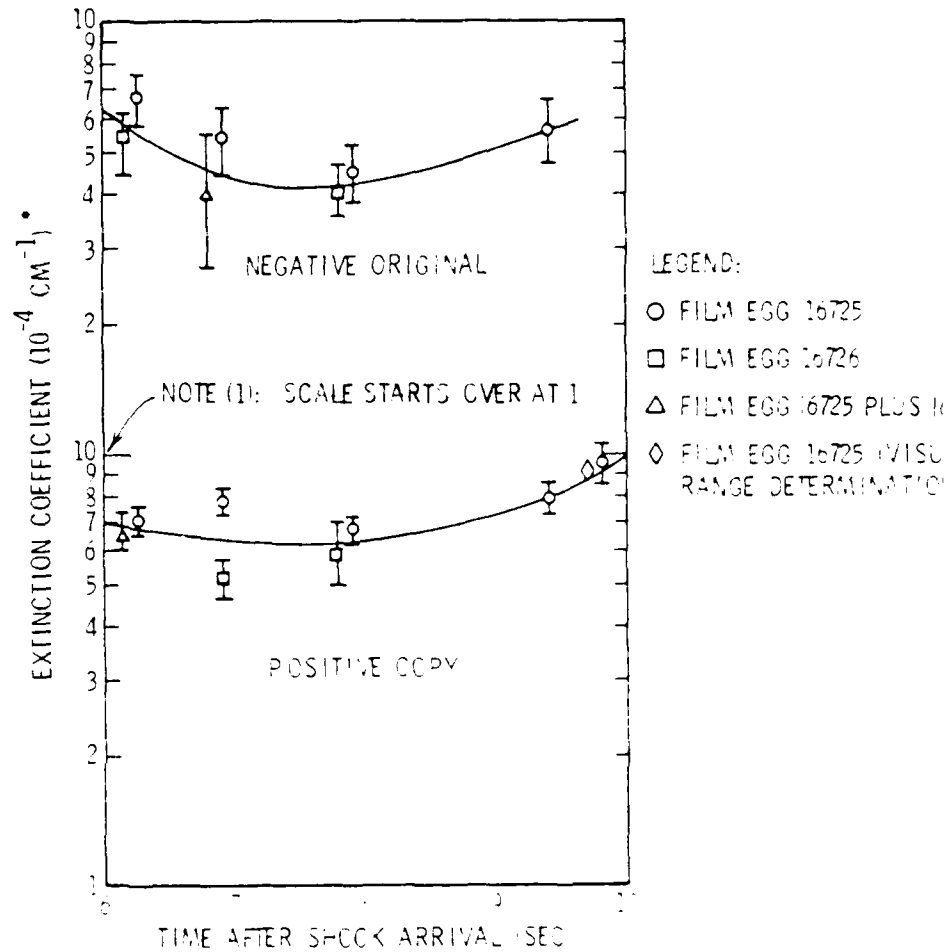
Figure 21. Extinction coefficient of dust vs. time as determined
by microdensitometer measurements of contrast attenuat[ion]
for lower left quadrant of image of boxcar in shot CR.

*Note (2): Dust concentration (GM/CM^3) = (1.26×10^{-2}) × extinction
coefficient (based on Equation 9 with HAPOL 325 particle
size distribution).

Note (3): Some adjacent data points have been slightly displaced to
avoid overlap. However, they correspond to exactly the
same times.

approach, which eliminated the use of C_o, was taken. In this case the attenuation in contrast observed in moving the viewpoint from A to B wa used to arrive at the extinction coefficient. Here β_s is obtained from

$$\frac{C_B}{C_A} = \exp\ (-\beta_s R_{AB}) \qquad , \qquad (15$$

where C_B and C_A are the contrasts of the lower left boxcar quadrant as measured from frames photographed at the same time by cameras B and A, respectively, and R_{AB} is the distance between A and B, namely 24 meters The resulting extinction coefficient values, denoted by triangles in Figure 21, are seen to corroborate the other data.

Finally, the diamond shaped data point on the lower curve (c of Figure 21 is the value of the extinction coefficient deduced in Section 3 strictly from visual threshold determination. It is notewort that this determination was made prior to and independently of the micr densitometer measurements.

5.3   H AND D CURVE CONSIDERATIONS

Up to this point no consideration has been given to the application of H and D curve corrections in arriving at the desired brightness levels from the microdensitometer transmittances. No such corrections were applied because, at the time of writing, this data had not been located for the films under examination. However, the followin discussion will provide assurance that, at least in so far as the origin negative is concerned, such corrections to the brightness contrast level and to the resultant extinction coefficient and dust concentration value are likely to be insignificant.

In the first place it is quite reasonable to assume that the exposure latitude of the emulsion employed was such that, in the moderate exposure region considered in the selected GRABLE films, the characteristic curve is linear (Reference 16). For this situation we have

$$D = \Gamma \log_{10}(Bt) + D_0 \quad , \tag{16}$$

where D is the film density, Bt is the exposure (with t being the exposure time), and Γ is the slope of the linear portion of the curve. But the density as determined by the microdensitometer is

$$D = \log_{10}(1/T) \quad , \tag{17}$$

where T is the measured transmittance. Combining Equations 16 and 17 we obtain

$$1/T = Kt^{\Gamma} B^{\Gamma} \quad , \tag{18}$$

where K and t are constants. In terms of the ratio of the reciprocal transmittance of the image of the object to that of the background we have

$$(1/T_{ob})/(1/T_{bg}) = t_{bg}/t_{ob} = (B_{ob}/B_{bg})^{\Gamma} \quad . \tag{19}$$

Now if Γ is assumed to be unity as it has up to now, then the object/background contrast is obtained directly from the transmittance as measured by the microdensitometer. That is,

$$C(\Gamma = 1) = (B_{ob}/B_{bg}) - 1 = (T_{bg}/T_{ob}) - 1 \quad . \tag{20}$$

If, however, Γ is not unity, then these same measured transmittances must be modified as follows to obtain the corrected value of contrast:

$$C(\Gamma \neq 1) = (T_{bg}/T_{ob})^{1/\Gamma} - 1 \quad . \tag{21}$$

But T_{bg}/T_{ob} is simply the uncorrected ratio, B_{ob}/B_{bg}. Therefore, the corrected contrast is given in terms of the uncorrected brightness ratio by

$$C_{corr.} = \left[(B_{ob}/B_{bg})_{uncorr.} \right]^{1/\Gamma} - 1 \quad . \tag{22}$$

Because the original film was processed under precision conditions, it is quite likely that the Γ of the negative does not vary more than five percent from unity in either direction (Reference 16). Assuming this maximum deviation, the corrected contrast can be determined from Equation 22 together with the uncorrected brightness ratios used to arrive at the negative original curves of Figure 19. When this is done, the curve obtained by averaging over all quadrants is found to differ by less than three percent from the $\Gamma = 1$ case, with the variation in extinction coefficient being in the same direction as the Γ variation. Thus, the extinction coefficient and corresponding dust concentration results obtained from analysis of the original negative can be considered very reliable apart from H and D corrections.

It is seen in Figure 19 that the positive copy curve is displaced upward from the negative original curve by an average of about twenty percent. This deviation can be explained on the basis of Equation 22 together with the assumption that the processing of the copy was performed in such a way as to produce an approximate forty percent enhancement in Γ.

Ordinarily, this is considered a very pronounced enhancement, but it can easily be accomplished in copying a film (Reference 17).

Moreover, such an enhancement of Γ is in accord with caveats given in Reference 18 as to the unadvisability of using the copies in photometric analysis. This reference states that the processing of the copies involved deliberate deviations from normal procedure in an attempt to maximize the usefulness of the films as regards to certain visual information of interest to the users at the time of filming. Thus, the GRABLE copies employed in the present study represent an extreme example of contrast distortion. In spite of this fact, it is reassuring that extinction coefficient and dust concentration results derived from the copy differ so little from results derived from the original[*].

---

[*] It has been brought to the attention of the authors that the negative employed in the measurements actually was not the original but a copy thereof (Ref. 19). Regarding the acceptability of the use of this negative the authors have consulted with an individual who was principally involved with EGG in the XIS photography, was the inventor of the film used, and is recognized as a foremost sensitometrist (Ref. 20). It is his opinion that the copying procedure in this case was sufficiently well controlled that the characteristic curve of this copy is very nearly the same as that of the original. He is, therefore, of the opinion that, for the present considerations (i.e. brightness ratio measurement as opposed to absolute brightness), the use of this copy should for all practical purposes give the same results as the original negative would give.

6.0 TEST PLAN

6.1 INTRODUCTION

The contrast attenuation technique for deducing dust concentration levels from NTS films shows great promise for extracting useful data from the existing film library. In addition to providing a new type of measurement from these archived films, the technique can also be used to normalize existing computer codes and/or assist the phenomenology modelers in their formidable task of describing dust environments. However, unless the accuracy, limitations and sensitivities of the technique are quantitatively known, the resulting dust concentrations will be viewed with a skeptical eye by any potential user. It was to dispel this skepticism and to provide concrete validation of the contrast attenuation technique that compelled us to recommend the series of tests given below.

As mentioned above, there exists a considerable number of films taken during atmospheric testing over an extensive period of time. Many of these films contain contrast attenuation information, i.e., a target and camera separated by a known distance and both enveloped by the sweep-up dust so as to partially or totally obscure the target at a known time. Unfortunately, for many of the films there exists little or no details which we could locate concerning photographic procedures, processing, and even camera settings. Rather than eliminate such films from the analysis effort altogether, it may be possible to at least bound the dust concentration derived from them by a careful and systematic study of the expected sensitivities to these parameters.

During the analysis effort reported herein, the nuclear tests that provided the data were TUMBLER-SNAPPER and UPSHOT-KNOTHOLE. Both of these test series have adequate documentation available to determine the necessary experimental configurations; therefore, we will model the validation experiments upon these specific cases. During the validation tests, we will also obtain data for use with films from other nuclear tests even where sufficient experimental details are lacking.

A number of known potential sources of error exist in the contrast attenuation method of determining dust concentration from NTS films. Table 5 lists these critical parameters. The intent of the validation experiments is to measure the sensitivity of the deduced dust concentration to each parameter as well as the cumulative errors.

Both the camera and film to be used for the validation experiments will be selected to match, as closely as possible, those used for the nuclear tests. In this way we will be able to perform specific tests under both laboratory and field conditions to determine their behavior and relate it to the nuclear test film data.

There are a number of parameters which affect the film data that relate to actual test conditions. These are the background luminance, dust particle size distribution, and particle absorption and scattering relations. We will measure the background luminance, dust density, particle size, and the index of refraction for the dust particles actually encountered during the photographic sessions.

Table 5. Critical parameters affecting the accuracy of the contrast attenuation method of determining dust concentration from NTS films.

PARAMETER	SPECIAL ISSUES
CAMERA	SCATTERED LIGHT
	LENS SPEED
FILM	SPECTRAL RESPONSE SPEED PROCESSING ORIGINAL VS COPY OF FILM
BACKGROUND LUMINANCE	SPECTRAL CHARACTERISTICS TIME DEPENDENCE UNIFORMITY
PARTICLE SIZE DISTRIBUTION	SHAPE MAXIMUM AND MINIMUM SIZES
DUST ABSORPTION AND SCATTERING	INDEX OF REFRACTION SINGLE VS MULTIPLE SCATTERING
VISUAL RANGE	FILM VS EYE

6.2   TEST REQUIREMENTS

Validation of the contrast attenuation method will be done by reproducing as closely as possible, several NTS films from the TUMBLER-SNAPPER and UPSHOT-KNOTHOLE nuclear tests. Based on the test reports from these shots, the cameras and film used to produce the data in our dust density analyses are shown in Table 6.

There were three different types of cameras used to obtain data to which the contrast attenuation method was applied. These were the Mitchell, CSAP, and Eastman type; each one is described below.

Table 6. List of cameras and films used for determining dust concentration by contrast attenuation method.

TEST SERIES	CAMERA	SPEED (FRAMES/SEC)	FILM (TYPE)
TUMBLER-SNAPPER	MITCHELL	35	918
	FASTAX	700	918
UPSHOT-KNOTHOLE	BELL & HOWELL GSAP*	64	918

6.2.1   Mitchell Camera

The 35 mm High Speed Mitchell Camera is a precision unit capable of frame rates up to 128 frames/sec. Optically, it has the high resolution characteristics of professional motion picture equipment and was used for work between 24 and 100 frames/sec. Due to its large frame and fine resolution, it produced the maximum amount of information per frame of film and could easily incorporate a timing light mounted on the housing door to obtain timing marks on the side of the film.

Unfortunately, it is a large and expensive piece of equipment which restricted its use. Additionally, for nuclear testing, its large size made lead shielding more difficult. Therefore, the use of this camera was restricted to stations where quantitative information was desired and beyond the distances where shielding was considered necessary.

----

*Gun sight aiming point camera.

6.2.2   Fastax Camera

The 16 mm Fastax Camera used a continuous motion-rotating prism for very high speed movies. Although the image quality was poor, this camera gave a high exposure so that it was used when a low level of illumination was available.

6.2.3   GSAP Cameras

The Bell & Howell Gun Sight Aiming Point (GSAP) 16 mm Cameras were used for the majority of cases. Due to its small and compact size, they were easily shielded. Also, it was relatively inexpensive, with film magazines to facilitate loading.

The stock GSAP camera was furnished with a so-called universal focus lens which was not satisfactory for the type of photographic results desired. These were replaced by the manufacturer with a focusing lens and the camera modified to provide a "C" type lens mount. This change was made because the photography was not all at the effective infinity of the standard lens and also because the quality of the replacement lenses was much better than that of the original equipment.

The cameras as received from the manufacturers were placed on a collimator and the lenses shimmed to give the sharpest focus possible. New fiducial marks were then etched on the lens mounts. The results were most gratifying. Cameras which had given a resolution of approximatel 15 lines per millimeter and less before collimating started to give a consistent resolution of from 30 to 50 lines per millimeter. All cameras were then checked mechanically and electrically and minor adjustments made.

As a result of the care given them, the GSAP cameras operated extreme[l]
well mechanically on all shots and gave excellent resolution in the
field.

6.3   TEST REQUIREMENTS

The validation of the contrast attenuation method will be b[?]
on NTS films already existing. By duplicating as many of the actual t[?]
conditions as possible, new sources of errors between the validation
experiments and the NTS ones will be minimized. It is for this reason
that the choices of cameras, films and other equipment are constrained
For many choices, we could improve the quality of the data but since
a true reproduction is desired, this will not be done.

6.3.1   Equipment Requirements

6.3.1.1   Cameras and Film Requirements

A visit to the EG&G facility in Los Alamos was made to disc[?]
cameras, films and other details with personnel intimately familiar wi[?]
the NTS film data. It was their consensus that several problems exist
in faithfully reproducing the equipment used during the nuclear tests.

First, the GSAP cameras were all scrapped by EG&G many year[?]
a[?] and are not available. They did think it would be possible to loc[?]
other GSAP's and obtain them for our experiments, but this will require
search. As mentioned in Section 6.2.3, the lenses used on the GSAP ca[?]
were not the original ones supplied by the manufacturer but of better
quality with careful focussing done in the lab. Again, the actual len[?]
used are no longer available and new ones will be required.

A second problem mentioned by EG&G personnel was the procu
of Kodak Type 918 film used for all of the NTS films we have consider
This film is no longer manufactured by Kodak and would be difficult t
obtain. A careful study will be required to see if available films m
the 918's characteristics or if Kodak will manufacture Type 918 in su
cient quantity for our experiments.

Use of Mitchell and Fastax cameras for the validation expe
ments should not pose any problems. There are sufficient quantities
these cameras in EG&G's hands to satisfy our needs. Film for these c
should also be Type 918 so the previous remarks apply here as well.

6.3.1.2 Dust Measurements

A number of in situ dust measuring instruments will be use
to obtain time-resolved particle sizes. From this data, the particle
size distribution will be inferred and used to calibrate the contrast
attenuation dust concentration determination. The need for time-reso
measurements is to precisely match the time when a specific contrast
level is observed on the film for the different dust concentrations a:
ciated with different target-camera pathlengths.

We recognize that the measurement of in situ dust particle:
will be very challenging and will require careful planning. Although
there are a number of instruments available which are claimed to prov
such measurements, in fact, the choices available for our application
are very limited. Below we briefly describe several different instru-
ments currently available. A more detailed description is given in t:
Appendix.

An Electrical Aerosol Size Analyzer is manufactured by [text]
and has been extensively used in air pollution studies[1]. This in[strument]
ment gives size and number information for submicrometer aerosols [ques]
tions associated with this instrument include: 1) its use only f[or]
less than one micron in size, 2) its requirement for approximatel[y]
minutes to process a sample (which eliminates time-resolved data)
3) its fairly expensive cost, (i.e., $20-30K per instrument).

Another instrument available is an optical interferomet[er sys]
tem built by UTSI and Spectron and called a Particle Sizing Inter[ferometer]
(PSI)[2]. It obtains in situ particle size, velocity, and number d[ensity]
vs time. The particle sizes that can be measured extend over a r[ange]
20:1 with the mean size easily adjustable from about 1μm to milli[meters]
Thus, a very broad range can be covered by using several instrume[nts].
An advantage claimed for this instrument is that it is non-invasi[ve]
does not disturb the flowfield. The main disadvantages are the s[mall]
dust volume and the processing of the data. Questions have arise[n]
concerning the uniqueness of the resulting particle sizes. For t[hose]
in which the particle size range is known that is not a serious p[roblem]
but for the general case of an unknown size distribution, it coul[d be]
a limiting factor.

The final instrument which we will discuss is the Forwa[rd]
Scattering Spectrometer Probe built by PMS[3]. It samples the part[icles]

(1) TSI, Incorporated, St. Paul, Minnesota.
(2) University of Tennessee Space Institute, Tullahoma, Tennessee.
(3) Particle Measuring Systems, Boulder Colorado.

air by using a flowtube placed in the free airstream. Time resolv

measurements are obtained and by selecting the appropriate compone

different size ranges can be measured. Many of these instruments

been used for measuring dust concentration and particle size distr

in a variety of field tests.

We have tentatively chosen the PMS instruments for our v

tion experiments. Several of these instruments are available for

any DOD sponsored test. In addition, prior to field tests, we pla

conduct trials to improve the data from these instruments and enha

their credibility for this application.

6.3.2   Analysis Requirements

As with any major test program, the requirements for ana

fall into two general areas: Predictions and Test Data Processing

will discuss each of these below.

6.3.2.1 Test Predictions

Prior to conducting tests that validate the contrast att

tion method of determining dust concentration, several parameters

be defined or estimated. These include target-camera range, expe

dust concentrations, duration of dust cloud, motion of dust cloud,

pressure expected if near an explosion, and luminance of target a

background. After considering these factors, a test plan will be

produced specifying all of the locations for cameras and targets

well as any necessary protection. Accurate predictions of the par

eters become mandatory for large-scale in tests where only a sin

event occurs. A preferable method would be to conduct sma

which can be repeated several times so as to optimize the

eters. Then using these results and some scaling relation

confidently predict the values for the larger HE test.

6.3.2.2 Data Analysis

Data from the validation experiments will fall

categories. First, there will be films of targets from wh

attenuation information will be obtained. Second, there w

particle measurements taken at the same location and time

data to provide absolute calibration of the dust concentrat

by the contrast attenuation method.

Film processing and analysis will conform to the

as much as possible. We will use the capabilities and fac

EG&G laboratory in Los Alamos to insure maximum consistenc

processing. No difficulties are expected in reproducing th

conditions since many of these films were processed in thi

by the same personnel.

For a quick-look capability, we may assemble a

cessing facility that can be transported and used at the t

used, this facility will provide pre-test calibration and

of various test parameters.

Analysis of the dust particle data will depend

mentation chosen to make the measurements. In any event,

be used to deduce dust concentration, particle size distrib

temporal characteristics. Also, dust samples will be analy

determine index of refraction data for use in computing the

coefficient.

6.3.3   Test Facilities

A faithful reproduction of the NTS film data req

atmospheric nuclear burst. Barring this, the next best sin

be a high-yield HE test designed to produce blast condition

those of an equivalent field nuclear test. Such a simulati

at the HILL RACE III field test. We propose to conduct th

validation test at the HILL RACE III with earlier setup and c

field test at a convenient dusty site such as NTS.

6.3.3.1

Prior to the HILL RACE III Test, a series of field

will be conducted at the Nevada Test Site or other convenie

locations. The intent of these tests is to thoroughly explo

cameras, films, and other instruments and optimize the diffe

or at least determine their effects. Depending upon the cor

this site, we may obtain contrast attenuation data, but no

simulate realistic dust clouds will be made. Thus we do no

see an enveloping dust cloud around the camera and target a

although we may kick up dust between them using a truck so as to obscure the visual path while photographing the target. In this way, by having the opportunity to test different configurations under controlled conditions, we will be able to prepare for MILL RACE with some confidence in our ability to obtain all of the required data.

6.3.3.2 MILL RACE

The planned validation experiment will be conducted at the MILL RACE HE Test in late summer/fall of 1981. At the present time, there is no information available to us for any detailed test planning. However, based on similar tests conducted in the recent past, we can speculate on some of the environments to be expected at MILL RACE.

First, the location is to be at the White Sands Missile Range in New Mexico. Depending upon the specific test site, we may not create a dust cloud composed of similar size and type of dust particles as was done at the NTS shots. This may or may not be important to our test. The previously described field tests will be used to determine any such sensitivities.

We expect that our location at MILL RACE will be somewhere around the 10-20 psi distance from GZ. This will ensure an adequate dust cloud and also adequate dust concentration within the cloud. Our cameras and targets will be placed at approximately the same distance from GZ so as to produce a uniform sweep-up dust cloud between them. Hardened camera and target sites will be required as will protection for the dust particle instruments.

The cameras will have film lengths suitable for the expected test duration. This may range from one to several minutes depending upon the predicted dust cloud's behavior. For both the GSAP and Mitchell cameras, the required film lengths will be about 200 ft/min, while the Fastax camera will require considerably longer lengths if used at the very high speeds shown in Table 6.

7.0 CONCLUSIONS AND RECOMMENDATIONS

It is concluded from the preceding study that measurement of photographic contrast attenuation is a feasible means of ascertaining the extinction coefficient and the concentration of shock-entrained dust. The contrast attenuation measurements can be performed visually at specific instants of time at which an object at a known distance from the camera is at the threshold of visibility. Alternatively, and more generally, measurements at times other than the instant of threshold may be obtained with the aid of a microdensitometer.

Extinction coefficient results obtained by visual means were found to be in excellent agreement with those obtained using the calibrated instrument. Moreover, consistency of the method was verified when results obtained for two different test shots having roughly equivalent scaled test conditions were found to be in close agreement. Further consistency was established when measurements on simultaneous frames of the same object photographed from different distances yielded closely agreeing results.

Microdensitometer measurements were made on selected frames of the original negative, and identical measurements were performed on the same frames of a positive copy. Due to precision processing of originals, the results obtained from them are expected to be very reliable. However, the study indicated that even copies, which were processed carelessly or with deliberate contrast distortions, are capable of yielding extinction coefficient values falling within twenty percent of those determined from an original.

Dust concentration levels were calculated from the measured extinction coefficient values using several (in some cases, arbitrary) choices of particle size distribution. The resulting concentration was found to be quite sensitive to variations in the distribution, implying that care must be taken to correctly specify the distribution. Fortunately, no uncertainty in the calculated dust concentration is introduced by this sensitivity since reliable experimental particle size distribution data for shock-entrained dust from an NTS shot is available.

A number of potential error sources associated with the contrast attenuation technique were identified in the study. With regard to visual determination of threshold contrast the most prominent error source is that resulting from variation among individual observers in the eye's threshold level. This source of error is eliminated, however, when the alternate approach of measuring the contrast with a microdensitometer is taken. A potential error source that remains, however, is the possible lack of fidelity of contrast reproduction through the photographic process. Such a lack of fidelity was experimentally demonstrated in the study for the case of fog, but it is impossible to extrapolate the results of this experiment to the dust and the particular film and processing associated with the NTS tests.

In view of the established practicability of the contrast attenuation technique it is recommended that it be fully exploited through a program of comprehensive measurements on all suitable NTS films. By this means scaling laws can be constructed which relate the deduced dust concentrations to all relevant parameters (e.g., yield, HOB, range, altitude, time, etc.). Concurrently, sw. up dust code calculations

82

should be performed for comparison purposes. It is further recommended that a similar comprehensive measurement program be carried out for films depicting pre-shock dust. Also, any possible refinements to the theoretical machinery for reducing this comprehensive set of contrast measurements to dust concentration data should be undertaken concurrently. For instance, refinement of Mie cross section calculations to take into account the entire visible spectrum and the non-sphericity of the dust particles should be undertaken. Furthermore, in order to be able to correct for any deviations in contrast which may be introduced by the photographic process, the extent of these deviations should be ascertained by means of the simulation experiment discussed in Section 6.

REFERENCES

1. Liner, R. T., Powers, J. T., Shannon, J. A., and Versteegen, P. L., "Nuclear Precursor Phenomenology and Sweep-Up Dust Cloud Model Development," DNA3781F, November 1975.

2. Dudziak, W. F. and Lad, P. V., "Thermal Dust Measurements from Nuclear Detonation Photography," RM78-ISI101, Information Science, Inc., November 1978.

3. Houghton, H. F. and Radford, W. H., "On the Measurement of Drop Size and Liquid Water Content in Fogs and Clouds," Pap. Phys. Oceanog. Meteorol., 6, No. 4, Mass. Inst. Tech., 1938.

4. Platt, C. M., "Transmission of Submillimeter Waves Through Water Clouds and Fogs," J. Atmos. Sci., 27, 1970.

5. Eldridge, R. G., "The Relationship Between Visibility and Liquid Water Content in Fog," J. Atmos. Sci., 28, 1971.

6. Kumai, M., "Arctic Fog Droplet Size Distribution and Its Effect on Light Attenuation," J. Atmos. Sci., 30, 1973.

7. Middleton, W. E. K., Vision Through the Atmosphere, University of Toronto Press, 1952.

8. Keith, J. R., "Nuclear Weapons Thermal Radiation Phenomena," Volume 1, Chapter 2, K-73-534(R), Kaman Sciences Corp., September 1973.

9. Blackwell, H. R., "Contrast Thresholds of the Human Eye," J. Opt. Soc. Am., 36, 1946.

REFERENCES (Continued 1)

10.   De Luisi, J. J., et al., "Results of a Comprehensive Atmospheric
        Aerosol-Radiation Experiment in the Southwestern United States,"
        J. Appl. Meteorol., 15, 1976.

11.   Patterson, E. M., Gillette, D. A., and Stockton, B. H., "Complex
        Index of Refraction Between 300 and 700 nm for Saharan Aerosols,'
        J. Geophys. Res., 82, 1977.

12.   Schuerman, D. W., Editor, Light Scattering by Irregularly
        Shaped Particles, Plenum Publishing Company, New York, 1980.

13.   Powers, J. T., Mansfield, J. E., and Liner, R. T., "Precursor
        Dust Cloud Model and Thermal Layer Development," DNA3876F,
        December 1975.

14.   Gordon, M. G., Stoudt, J. F., and Francis, A. B., "Dust Density
        Versus Time and Distance in the Shock Wave," Operation
        Teapot-Project 1.13, Report to the Test Director, WT-1113,
        June 1957.

15.   Bouton, E. H., Elder, C. S., Kemper, J. S., and Wilsey,
        E. F., "Pre-Shock Dust," Operation Tumbler-Project 1.9,
        Report to the Test Director, WT-519, October 1952.

16.   Private Communication with Emery Praither, DNA Field Command,
        July 3, 1980.

17.   Private Communication with Al Greco, TVC Film Producers and
        Copiers, New York, N. Y., July 7, 1980.

18.   Greer, W. R., and Dukes, E. F., "Technical Photography,"
        Operation UPSHOT-KNOTHOLE-Project 9.1, WT-779, p. 31.

REFERENCES (Continued 2)

19.   Private Communication with Walter Dudziak, September 20,
        1980.

20.   Private Communication with Charles Wyckoff, November 6,
        1980.

APPENDIX

DUST MEASUREMENTS FOR CAT[*] VALIDATION

Contributed by Dr. J. E. Cockayne)

The requirements for dust data include average mass concentra
tion along the optical path, the complete PSD[**] for the effective-scatt

spherical size, the index (complex) of refraction, the complete PSD for

the effective-mass-spherical size, and the specific gravity. These dat

are needed for validating the CAT using equation (9). Fortuitously,

the PSD is weighted by "almost" the same moments above 0.1 micrometer

so absolute accuracy is partially alleviated by the ratioing of the two

integrals over the PSD. A decreasing specific gravity, for increasing

size, is possible due to the transition from grains to aggregates/

agglomerates so the third power could also be effectively reduced and

get the powers closer.

The primary devices for measuring the path averaged dust dens

include microwaves, nuclear radiation and multiple point samplers of

various designs. Microwave phase shifting has recently been applied by

SRI International to cases with vastly larger amounts of mass along the

path (g/m^2). Thus complete reevaluation would be required as well as

probably more sophisticated instrumentation. (The wavelength could be

decreased from UHF but it must be kept large enough to keep all partic

in the Rayleigh scattering regime).

[*] Contrast attenuation technique

[**] Particle size distribution

Various nuclear gages are proven but none is currently config

for this application. Beams of gamma rays, x-rays, beta particles and

SAI proprietary hybrid are available but need a sensitivity analysis for

these distances and densities, as well for the other conditions such as

eventual blast hardening. The multiple point approach may be synergist

because of the need for more detailed data (i.e., PSD) along the path.

The need for collected particles, to measure both specific gravity and

index of refraction, can also influence the likely sensor for multiple

stations.

The PSD data can be automatically measured by techniques usin

an electric field, aerodynamic drag and at least two optical interactio

for sorting/sizing. Unfortunately, the large range of number concentra

limits the effectiveness of any single probe to approximately a factor

of 10 to 20 in size, unless the temporal and/or dimensional resolution

degraded. These time resolved data can be supplemented by case type

analyses in a laboratory using dust collected by filters or coated

impactors. Filters might also be synergistically combined with one PSD

device for multiple station data. That possibility is discussed in the

following approach.

An aspirated system can be assembled that obtains both densit

and the weighted modes of the PSD. The PSD measurement by the forward

Scattering Spectrometer Probe* (FSSP) uses aspiration to pull the dusty

air through a laser beam. The FSSP's flowtube is sampled by the laser

at its center so particles that are agglomerated together will not be

*Manufactured by Particle Measuring Systems, Inc. of Boulder, Colorado

broken up until after they are sized and enter the aspirator tan

of the tube system. A filter can easily be added to the outlet

(integrated) density measurements. By normalizing the FSSP's PS

output to the filter's mass gain, the time varying density can b

recovered. The FSSP can be automatically operated at approximat

0.5, 1, 2, or 3 micrometer (diameter) threshold and resolution s

nating between the 0.5 and 3 settings will produce good PSD data

1 and 50 micrometers, which should definitely include the mode o

differential mass. The mode of the differential scattering area

occur at a small size but not significantly below 0.5 micrometer

the falloff of Q (Figure 10). Because a single in-situ experime

(TEAPOT MET) had its number median diameter at 1.2 micrometer, t

median will definitely be larger if that empirical PSD is accura

mass median diameter was 15 micrometers. The factor of 20 small

median for TUMBLER-SNAPPER DOG (Table 4) thermal blowoff (pre-sa

implies that the FSSP would need to be replaced by its clone for

sizes; or an additional probe added but that doubles the require

acquisition interfaces in a multiple station configuration.

The path averaged/density calculated from multiple sta

would probably use many extra filter stations in order to accura

represent the variation(s) along the path. In that case, the sa

stands should be painted black in order for the photography to p

density estimates for many short paths that are more uniform.

Other PSD instruments of interest are the Electrical A

Analyzer (EAA)* and the Particle Sizing Interferometer (PSI)**.

sizing technique of the EAA is limited to aerosol sizes which is

unsuitable here, based on the TEAPOT MET PSD. Another disadvant.

the regular EAA system is the two minute processing time for eac

which precludes time resolved PSDs.

The PSI uses a projected bright/dark fringe pattern pr

laser beam interference for a particle to traverse. Under very

conditions, the wide bandwidth signal can be processed to obtain

area and both particle "diameter" and velocity transverse to the

lines/bands. The inherent interferometric principle makes this

very sensitive to any change(s) in the electrical mechanical or

subsystems. Thus the PSI is not directly compatible with the lo

unattended operation dictated by the large HE (MILL RACE) test p

The advantage of the PSI is that it is non-invasive, which may b

for highly turbulent precursed shock waves. But the photographi

integrates along a path so it eliminates any direct sensitivity

associated inhomogeneities. Despite the flowtube of the FSSP, t

diagnosed air volume is totally sheathed by air so the particles

unaffected until after sizing. The principle of the FSSP is ot

scattering in the forward direction so it is also sensitive

scattering area of the particle despite the fact that the ou

formatted as diameter.

A final PSD instrument for consideration is the a

cascade impactor. This sensor uses aerodynamic sorting with

"micro-balances" (QCM)* at each stage/impactor for real time

the PSD --by differentiating the cumulative mass on each impa

Because sensitivity is controlled by the integrated masses,

is almost inverse in time to that desired for the shock entra

layer. Other disadvantages include the mass carry-over from

stages as they saturate and the conversion from aerodynamic

optical (scattering) area for this application.

*Manufactured by California Measurements Inc., or Sierra Rad
and Berkeley (Celesco) Instruments, Inc. of Irvine, Califor

DEPARTMENT OF DEFENSE

Assistant to the Secretary of Defense
Atomic Energy
        ATTN: Executive Assistant

Defense Advanced Rsch Proj Agency
        ATTN: TIO

Defense Communications Agency
        ATTN: CCTC

Defense Intelligence Agency
        ATTN: DT-2, T. Dorr
        ATTN: RD-4B
        ATTN: DT-1C
        ATTN: DT-2

Defense Nuclear Agency
        ATTN:
        ATTN: NATA
        ATTN:
        ATTN: RAAE
        ATTN: STNA
   3 cy ATTN: SPAS
   4 cy ATTN: TITL

Defense Technical Information Center
   12 cy ATTN: DD

Field Command
Defense Nuclear Agency
        ATTN: FCTMOF
        ATTN: FCTMOT
        ATTN: FCTMD
        ATTN: FCPR
        ATTN: FCTT, G. Ganong

Field Command
Defense Nuclear Agency
Livermore Branch
        ATTN: FCPRL

Joint Chiefs of Staff
        ATTN: J-5 Nuclear Division
        ATTN: SAGA/SFD
        ATTN: J-3 Force Planning & Program Div
        ATTN:

Joint Strat Tgt Planning Staff
        ATTN: JLTW
        ATTN: JLA
        ATTN: JPTP, J. Clayton
        ATTN: JPST

DEPARTMENT OF THE NAVY (Continued)

Office of the Chief of Naval Operations
ATTN: OP 654E14, R. Blaise
ATTN: OP 654C3, R. Piacesi
ATTN: OP 65

Strategic Systems Project Office
Department of the Navy
ATTN: NSP-272
ATTN: NSP-2722, F. Wimberly
ATTN: NSP-273

DEPARTMENT OF THE AIR FORCE

Aeronautical Systems Division
Air Force Systems Command
2 cy ATTN: ASD/ENFTV, D. Ward

Air Force Flight Dynamics Laboratory
ATTN: FXG
ATTN: FBAC, D. Roselius

Air Force Geophysics Laboratory
ATTN: LY, C. Touart

Air Force Materials Laboratory
ATTN: MBE, G. Schmitt
ATTN: MBC, D. Schmidt
ATTN: LLM, T. Nicholas

Air Force Rocket Propulsion Laboratory
ATTN: LKCP, G. Beale

Air Force Systems Command
ATTN: SOSS
ATTN: XRTO

Air Force Technical Applications Center
ATTN: TF

Air Force Weapons Laboratory
Air Force Systems Command
ATTN: NTYV, A. Sharp
ATTN: HO, W. Minge
ATTN: DYV
ATTN: NTES, K. Filippelli
ATTN: SUL
ATTN: DYV, E. Copus
2 cy ATTN: NTO

Arnold Engineering Development Center
Air Force Systems Command
Department of the Air Force
ATTN: Library Documents
ATTN: DOOP, G. Cowley

Ballistic Missile Office
Air Force Systems Command
ATTN: MNN
ATTN: MNRTE
ATTN: MNNR
2 cy ATTN: MNNXH, Blankinship
3 cy ATTN: MNNXH, Allen

Deputy Chief of Staff
Operations Plans and Readiness
Department of the Air Force
ATTN: AFXOOSS

DEPARTMENT OF THE AIR FORCE (Continued)

Deputy Chief of Staff
Research, Development, & Acq
Department of the Air Force
ATTN: AFRD
ATTN: AFRDQI

Foreign Technology Division
Air Force Systems Command
ATTN: SDBS, J. Pumphrey
ATTN: TQTD
ATTN: SDBG

Headquarters Space Division
Air Force Systems Command
ATTN: RST
ATTN: RSS

Headquarters Space Division
Air Force Systems Command
ATTN: AFML, G. Kirshner

Strategic Air Command
Department of the Air Force
ATTN: XPFS
ATTN: XPQM
ATTN: XOBM
ATTN: DOXT

DEPARTMENT OF ENERGY

Department of Energy
ATTN: OMA/RD&T

OTHER GOVERNMENT AGENCY

Central Intelligence Agency
ATTN: OSWR/NED

DEPARTMENT OF ENERGY CONTRACTORS

Lawrence Livermore National Laboratory
ATTN: L-262, J. Knox
ATTN: L-92, C. Taylor
ATTN: L-125, J. Keller
ATTN: L-24, G. Staihle

Los Alamos National Scientific Laboratory
ATTN: MS 670, J. Hopkins
ATTN: R. Dingus
ATTN: J. Taylor
ATTN: R. Thurston
ATTN: J. McQueen
ATTN: D. Kerr

Sandia National Laboratories
ATTN: M. Cowan
ATTN: A. Chabai

DEPARTMENT OF DEFENSE CONTRACTORS

Acurex Corp
ATTN: C. Powars
ATTN: C. Nardo
ATTN: R. Rindal

Aerojet Solid Propulsion Co
ATTN: R. Steele

DEPARTMENT OF DEFENSE CONTRACTORS (Continued)

Aeronautical Rsch Assoc of Princeton, Inc
    ATTN: C. Donaldson

Aerospace Corp
    ATTN: R. Crolius
    ATTN: J. McClelland
    ATTN: W. Barry
    ATTN: H. Blaes

Analytic Services, Inc
    ATTN: J. Selig

APTEK, Inc
    ATTN: T. Meagher

AVCO Research & Systems Group
    ATTN: J. Stevens
    ATTN: W. Broding
    ATTN: Document Control
    ATTN: J. Gilmore
    ATTN: A. Pallone
    ATTN: W. Reinecke

Battelle Memorial Institute
    ATTN: M. Vanderlind
    ATTN: E. Unger
    ATTN: R. Castle

Boeing Co
    ATTN: M/S 85/20, E. York
    ATTN: B. Lempriere
    ATTN: R. Dyrdahl
    ATTN: R. Holmes

California Research & Technology, Inc
    ATTN: K. Kreyenhagen
    ATTN: M. Rosenblatt

Calspan Corp
    ATTN: M. Holden

Effects Technology, Inc
    ATTN: R. Parisse

General Electric Co
Space Division
    ATTN: C. Anderson
    ATTN: D. Edelman
    ATTN: G. Harrison

General Electric Co
Re-Entry & Systems Div
    ATTN: P. Cline
    ATTN: B. Maguire

General Electric Co—TEMPO
    ATTN: DASIAC
    ATTN: B. Gambill

General Research Corp
    ATTN: J. Mate

Harold Rosenbaum Associates, Inc
    ATTN: G. Weber

Hercules, Inc
    ATTN: P. McAllister

DEPARTMENT OF DEFENSE CONTRACTORS (Continued)

Institute for Defense Analyses
    ATTN: J. Bengston
    ATTN: Classified Library

Kaman Sciences Corp
    ATTN: D. Sachs
    ATTN: J. Hoffman
    ATTN: J. Keith
    ATTN: F. Shelton
    ATTN: J. Harper

Lockheed Missiles & Space Co., Inc
    ATTN: F. Borgardt

Lockheed Missiles & Space Co., Inc
    ATTN: R. Walz

Los Alamos Technical Associates, Inc
    ATTN: C. Sparling
    ATTN: P. Hughes
    ATTN: J. Kimmerly

Martin Marietta Corp
    ATTN: E. Strauss

McDonnell Douglas Corp
    ATTN: J. Garibotti
    ATTN: L. Cohen
    ATTN: P. Lewis, Jr
    ATTN: H. Berkowitz
    ATTN: R. Reck
    ATTN: H. Hurwicz
    ATTN: G. Johnson
    ATTN: E. Fitzgerald
    ATTN: D. Dean

National Academy of Sciences
    ATTN: D. Groves

Pacific-Sierra Research Corp
    ATTN: G. Lang
    ATTN: H. Brode

Physics International Co
    ATTN: J. Shea

Prototype Development Associates, Inc
    ATTN: J. Dunn
    ATTN: J. McDonald
    ATTN: M. Sherman

R & D Associates
    ATTN: C. MacDonald
    ATTN: P. Rausch
    ATTN: W. Graham, Jr
    ATTN: J. Carpenter
    ATTN: F. Field
    ATTN: P. Haas

Rand Corp
    ATTN: R. Rapp

Rockwell International Corp
    ATTN: B. Schulkin
    ATTN: G. Perroue

Science Applications, Inc
    ATTN: G. Burghart